COMPARISON OF THE EFFECTS OF MIXING AND INFILTRATION OF HYDROXYAPATITE WITH CALCIUM NITRATE

by

Jiapeng Qi

Bachelor of Engineering, Materials Science & Engineering, Jiangsu University, 2014

Submitted to the Graduate Faculty of

Swanson School of Engineering in partial fulfillment

of the requirements for the degree of

Master of Science

University of Pittsburgh

2016

UNIVERSITY OF PITTSBURGH

SWANSON SCHOOL OF ENGINEERING

This thesis was presented

by

Jiapeng Qi

It was defended on

April 1, 2016

and approved by

Ian Nettleship, Ph.D., Associate Professor

Department of Mechanical Engineering and Materials Science

Qing-ming Wang, Professor

Department of Mechanical Engineering and Materials Science

Jung-kun Lee, Ph.D., Associate Professor

Department of Mechanical Engineering and Materials Science

Thesis Advisor: Ian Nettleship, Ph.D., Associate Professor, Department of Mechanical Engineering and Materials Science

COMPARISON OF THE EFFECTS OF MIXING AND INFILTRATION OF HYDROXYAPATITE WITH CALCIUM NITRATE

Jiapeng Qi, M.S.

University of Pittsburgh, 2016

Aimed to enhance the release of calcium ions to promote the cell expansion and growth of HSCs, a controlled gradient of CaO close to the exterior surface is designed in this study by infiltration. To establish a comparison with infiltration, an experiment of direct mixing HA with CaO is also conducted. XRD result revealed that the extra CaO incorporated into HA caused the formation of tetracalcium phosphate (Tetcp), which played a significant part in the formation of a surface precipitate and weight gain of the samples during immersion of the samples in saline. Infiltrated materials that showed less Tetcp formation showed weight loss and less surface precipitation.

TABLE OF CONTENTS

LIST OF TABLES

LIST OF FIGURES

ACKNOWLEDGEMENTS

I sincerely thank for my father funding me studying in the U.S purchasing my oversea study dream; thank for the meticulous care from my mother when I was stressed both in life and study; thank for my other family members being healthy the fact of which reassures me being abroad by myself.

I give my genuine appreciations to Zhang, Qinghao for the help in lab, in giving constructive suggestions at every-week meeting, and in thesis writing.

I give my wholehearted gratitude and respect to Dr. Nettleship for choosing me being his Master student, for patient instructions in academy, for earnest thesis revise. Such a kind and warm-heated academic advisor to follow with. It was his encouragement that made me feel I was making a progress every week. Both as an academic advisor and an individual person, I give all my respect for Dr. Nettleship.

I thank all my friends in Pittsburgh, thank you for being there available any time when I am in need. Have you by my side my graduate studying life has been enormously enriched. Such a wonderful time it is!

1.0 INTRODUCTION

Hydroxyapatite (HA) is the most important bio-compatible ceramics used for bone grafting[1,2,3] because its chemical composition closely resemble that of human bone. Hydroxyapatite is also a candidate scaffold material for culturing bone marrow cells, particularly the hematopoietic stem cells (HSC) that produce all the blood cells in the body and the cells that make up the immune system.

Sudies have suggested that could promote HSCs expansion and cell growth by influencing the signaling mechanism[4,5] of HSCs. Based on this fact a biphasic HA-CaO ceramic scaffolds is proposed here to enhance the release of calcium ions into HSCs culture medium. In this work, therefore, methods for incorporating CaO into HA to create calcium-rich HA were developed by both infiltration and mixing. While infiltration was conducted in samples after partial sintering at 1100 ℃, mixing was conducted by blending HA with calcium nitrate prior to calcination. The effect of the enhanced calcium content in the HA samples on phase distribution and the spatial distribution of phases were studied. The samples were then exposed to saline at room temperature for 0.5 hour, 1 hour, 1 day, 3 days, 1 week, 2 weeks, and 4 weeks periods. The effect of immersion on phase distribution, weight change and microstructure were examined.

2.0 BACKGROUND

In this section, the background knowledge pertinent to this thesis will be introduced. The topics include: regenerative medicine, bone marrow, calcium phosphate, sintering, and infiltration of ceramics with second phases. The first two subsections aim to point out the significance of this study, the third and fourth subsections are fundamental knowledge about the material and its processing while the last one is the technique used to introduce a functionally graded second phase.

2.1 REGERATIVE MEDICINE

Regenerative medicine is still in its infancy and yet to realize its true promise. As a research field it combines biomaterials molecular biology and bio-engineering with the aim of replacing or regenerating cells, tissues or organs to affect radical new clinical treatments. Regenerative medicine can be divided into two major areas including cell therapy and tissue engineering, which will now be introduced.

2.1.1 Cell Therapy

Cell therapy, cures the patient by injecting cellular materials into the patient's body.[6] These injected materials are usually living cells. The origin of cell therapy can be dated back to the 19th century when scientists attempted to inject animal cells into patients to treat and prevent the illness.[7] Although the result of these attempts were not positive, the idea was creative. Not until the mid-20th century did scientists discover that by using human cells instead of animal cells the rejection from the human immune system could be prevented. Probably the most successful transplantation at that time was bone marrow transplantation.[8]

There are two categories of cell therapy – mainstream medicine and alternative medicine. The first one, mainstream medicine, uses human cells while the second one, alternative medicine, uses animal cells. Intense research has been focused on mainstream medicine because of the potential therapeutic benefit. Compared with mainstream medicine, alternative medicine has much more potential danger and according to the American Cancer Society, this practice is not supported by any existent evidence of effectiveness.[6]

Stem cells play a big role in cell therapy and have been successfully utilized in certain clinical applications.[9] Since these cells are not differentiated into mature cells they commonly have the ability to differentiate into a number of useful cell types and also renew the stem cell population. This ability makes stem cells most desirable for cell therapy applications. In mammals like human, stem cells can be classified into two broad types, including embryonic stem cells and adult stem cells. The embryonic stem cells are isolated from the inner cell mass of blastocysts[10] while adult stem cells are found in specific microenvironments within the particular tissue or organ[11]. In comparison, adult stem cells are in general less versatile and flexible then embryonic stem cells for the fact that embryonic stem cells are primitive cells in form meaning

they have far potential ability to develop into almost every type of cell. Conversely, adult stem cells are of limited capability of developing into certain types of cells. With the development of researches, however, light has been given to adult stem cells. Using genetic reprogramming, adult-cell-generated pluripotent stem cells can be equivalent to embryonic stem cells. Sources of this type of embryonic-stem-cells equivalents can be found from human adult skin tissue.[12] Unfortunately, adult stem cells from other tissue origins to date still have the restriction in the types of cell that they are able to become and therefore are defined as multipotent stem cells instead.[13] These gene-reprogrammed adult stem cells are also named "Induced pluripotent stem cells", which was first practiced by Shinya Yamanaka's lab.[14] Shinya Yamanaka for this great breakthrough was awarded the 2012 Nobel Prize. The use of human embryonic material can be controversial because it needs to destroy an embryo. Embryonic stem cells can only be derived from embryos and it has been so far not feasible to create patient-matched embryonic stem cell lines. Strong immune suppressing drugs may need to use to conquer the rejection from the patient immune system. Whereas, regarding this aspect adult stem cells are in instances obtained from patients themselves thus having no risk of rejection. This is why adult stem cells are more often used in medical therapies, such as in bone marrow transplantation.

2.1.2 Tissue Engineering

Tissue engineering is born due to the serious shortage of transplant tissue for repair of defects or injuries that the body is not able to repair by natural processes. Tissue engineers are devoted to developing new approaches for promoting the growth and repair of the tissue. However, human tissue is never a simple, physical and mechanical requirements, biological complexity and biocompatibility issues continue to challenge scientists and make the development of tissue

engineering very slow. To date, only a few efforts have been clinically tested in patients[15]. These include skin wound repair, diabetes treating transplanted cells, and articular cartilage defects repair using chondrocyte implantation.

It is not easy to conceptually define tissue engineering but approaches of it can be categorized around five general applications[15]:

- Tissue engineering to extend conventional medical and surgical practices.
- Tissue engineering to provide new models for the study of human physiology.
- Tissue engineering to attempt to replace or supplement the cellular component of diseased tissues.
- Tissue engineering to control drug delivery by using cellular processes.
- Tissue engineering to involve control or regulation of the normal healing process.

As far as tissue engineering being concerned, porous three-dimension scaffold is reliable and has been extensively employed to offer tissues and organs appropriate bio-environment for regeneration whether it is implanted into the body to recruit cells and thereby form tissue or seeded with cells in-vitro allowing attachment and formation of tissue prior to being implanted in the body. There will be a sub-section behind, section 2.2.2, to introduce both bio-reactors and scaffolds.

2.2 BONE MARROW

Bone marrow, which occupies the center of large bones, is a flexible tissue and is normally associated with hematopoiesis, the process of creating new blood cells in the body which will be

discussed in the following subsection 2.2.1. To relate bone marrow with hematopoiesis, firstly it is necessary to understand the components and the architecture of bone.

Large bones, such as femur, consist of two distinct types: cortical (compact) bone and cancellous or trabecular (spongy) bone. A brief sketch of bone showing these two is displayed in Figure 2.1[16]. Cortical bone is a dense cylinder accounting for 80% mass of bone but has a much lower surface area than cancellous bone because of its low porosity. Cancellous bone, accounting for approximately 20% of the total mass of the skeleton is commonly located at the ends of long bones and has an open porous structure shown in Figure 2.2[17]. While the cortical bone provides the high strength, high stiffness, and appropriate skeletal properties to shield the central bone marrow cavity, the cancellous bone houses the blood vessels and bone marrow itself. The porosity of cancellous bone ranges from 30 - 90% and so its surface area is ten times higher than that of compact bone and its mass is only one fourth of that of compact bone.

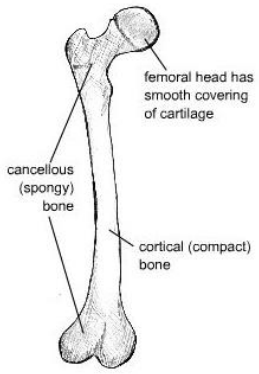

Figure 2.1 Morphological sketch of bone

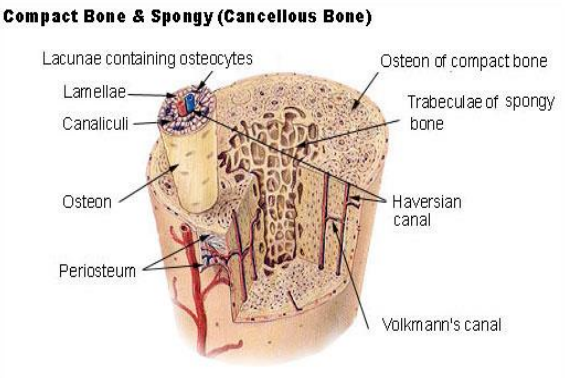

Figure 2.2 Bone structure.

Other than cells bone is composed of collagen fibers and small-crystal of the inorganic bone mineral. Living bone (in the body) also contains water ranging from 10% to 20% of its total

weight. Approximately 60 – 70% of the dry mass is the mineral phase of bone. The remainder of the material is mostly collagen, which has a triple helical structure and is the main fibrous protein in the human body[16]. Other substances such as proteins and inorganic salts account for a much smaller fraction of the bone mass. The main component of bone, the inorganic mineral phase can be approximated as $Ca_{10}(PO_4)_6(OH)_2$ or $Ca_5(PO_4)_3OH$, which will be discussed in section 2.3.

There are two types of bone marrow, which are called red marrow and yellow marrow showed in Figure 2.3[18]. The former one is mainly composed of hematopoietic tissue while the latter one is made up of fat cells. Both types of bone marrow contain a high density of blood vessels and capillaries, due to the fact that it is an organ and perfusion is important to the cellular processes occurring there. Before birth, in the fetus, all bone marrow is red. Then as the fetus develops some of the red bone marrow is converted into yellow marrow. As far as an adult is concerned, red marrow takes up around half of the bone marrow cavity. Under the condition of blood loss, yellow marrow can be converted back to red marrow in order to increase the production of blood cells.

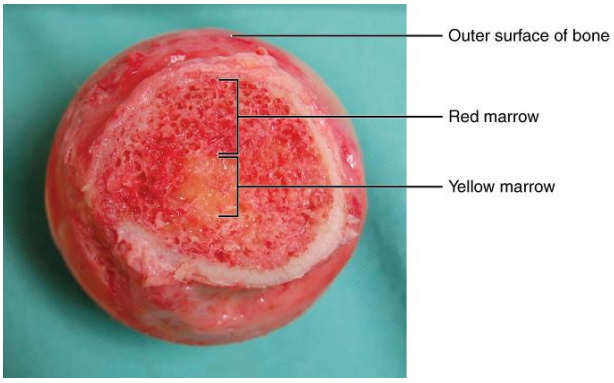

Figure 2.3 Two types of bone marrow

In humans, red blood cells are produced in the hematopoiesis process by red bone marrow. In fact, the production of blood cells by bone marrow is extremely high, approximately 500 billion blood cells are produced per day in the adult human.[19] This amazing process is accomplished by using the vasculature of bone marrow as a conduit to the body's circulation.[20] Furthermore, bone marrow as another important role concerning the lymphatic system, by producing all the lymphocytes that support our immune system.[21] In the following parts, one of most important inhabitants, HSCs, and the human effort of trying to physically and biologically mimic the bone marrow environment will be introduced.

2.2.1 Hematopoietic Stem Cells (HSCs)

Hematopoietic stem cells (HSCs) were the first stem cells to be identified and they are the best-characterized of all the stem cell types.[22] HSCs have the ability to produce all types of blood cells persistently and while still the HSC population in the body and therefore sustaining hematopoiesis throughout life. They are located in specific microenvironments in the red bone marrow called the stem cell niche as shown in Figure 2.3.

Hematopoiesis is a process that is strictly regulated. Normally, it takes about 7 days for a committed cell to develop into a fully functional mature blood cell. When matured, it lives in blood circulation for around 100 - 120 days in a healthy individual.[23] Finally, it will be removed from circulation at the end its lifespan when it becomes senescent. Old ones die out while new ones are formed in the stem cell niche and released into the body circulation system. This is the nature rule how blood circulation functions. Figure 2.4[22] schematically shows the HSC differentiation path, which is organized hierarchically with a series of cell populations arranged in rank from stem cells to mature blood cells. Most importantly, the ability of HSCs to renew

suggests that, in theory, one stem cell is sufficient for establishment of the entire system. Therefore a small number of stem cells could be used to generate a range of blood cell products of the processes on renewal and differentiation could be reliably controlled.

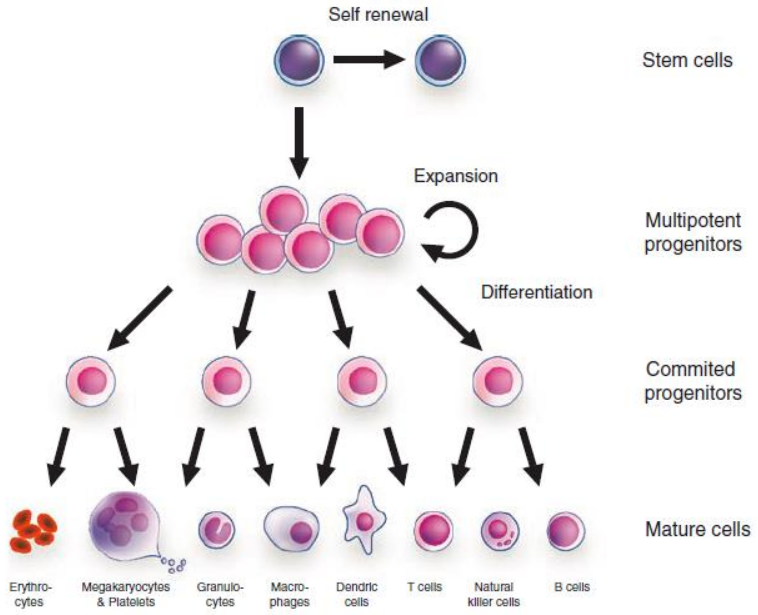

Figure 2.4 The hematopoietic system

Self-renew is the process of cell division that produces one or two daughter cells that are identical to the parental cell, which means this process copies the whole genome and epigenetic modifications. The potential of self-renewing and differentiating of the cell are both maintained throughout the division. Differentiation is the process through which cells become more functionally specialized. However, in this differentiating process the potential of self-renewal or some part of the multi-potency is lost. As the differentiation progresses from multipotent progenitor to committed progenitor, and finally to mature cell, the potential of the new differentiated cells is restricted progressively, which means afterwards the cells must evolve into

a certain direction. This process is called lineage commitment, in which progenitors are restricted into one particular lineage but not the other lineages. Generally, cells cannot reverse the sequences of differentiation.

Applications of Hematopoietic Stem Cells Stem cell therapy has been performed for more than 50 years to cure blood and immune system disorders.[24] Approximately half a million people have been treated with hematopoietic stem cell transplantation (HSCT), and the science of stem cell biology undergone rapid development. More recent refinement of these procedures have also lead to reductions in the morbidity and mortality that are associated with HSCT.

Within the classification of HSCT, generally there are two types: autologous and allogeneic. Autologous HSCT consists of removal, storage, and reinfusion of patient's own HSCs as an approach to restore the depleted bone marrow after high dose myeloablative therapy has been used to treat the cancer or blood disorder. Allogeneic HSCT includes transferring both mature and immature blood cells to a patient from sources such as the bone marrow or the peripheral blood of a sibling, relative, or a donor without consanguinity, as a means to restore the patient's bone marrow with a new immune system after conditioning regimen. The success of the allogeneic HSCT is compromised by the toxicity that comes from the conditioning regimens, graft versus host disease and opportunistic infections. In contrast, auto-HSCT is able to avoid the rejection by the patient's immune system and reduces the risk transplant failure or infection.

It is not always the case that every patient can be transplanted. The decision depends on individual circumstances and several other factors should be taken into consideration including the status of disease, age of the patient, prior treatments and responses. Even when all these factors are satisfied the availability of donor is a key issue question. Thus to solve this shortage

problem, efforts have been made to culture HSCs both in vitro and in vivo, in which case culturing related devices like bioreactors and scaffolds are indispensable.

2.2.2 Bioreactors and scaffolds

Applications of HSC in therapies are undoubtedly significant involving the replacement of blood and immune system. However, getting HSC applied in the clinic is very limited by the available amount of HSC. That is how in-vitro culture comes in becoming a heated topic in the field. To culture HSCs in-vitro, an appropriate bio-environment is needed for protecting and carrying the differentiation process from the progenitors. This specific environment is termed as HSC niche[5]. While HSCs need living environment which is niche, the niche itself needs carrier as well. This is not a simple case where a random container could resolve. There are rigid principles concerned with designing this niche carrier:

1) expansion of cells within the carrier should be rapid and controllable;
2) cell seeding effect should be enhanced on 3D scaffolds;
3) metabolization inside has to be efficient, such as oxygen and nutrients exchange;
4) physiological stimuli are provided.[25] Served as niche carrier is the bioreactor, a complicated device where all biological reactions take place, for example cell expansion, differentiation.

While scaffold by definition [26] is a temporary structure used to be a support in construction, maintenance, and repair. It is not the building construction that we are talking about in this content but bio-scaffolds that are engineered to make desirable cellular interactions happen contributing the formation of new functional tissues for clinical purpose.[27] A successful scaffold is required to have following properties[28]:

1) bio-compatible non-toxic surface that could promote cell adhesion and proliferation;

2) strong mechanical strength that is able to be used in implantation after the in-vitro culture;
3) porous structure to allow vascularization and nutrients diffusing between cells seeded in the matrix;
4) degradable but with non-toxic debris that could be either resorbed or excreted by the body and the best degrading rate is to match the new tissue formation;
5) manufacturing viable to scale-up.

However, there are still problems with using scaffolds. Among these challenges, the most significant one is difficult to get tissue to form in the interior of large scaffolds because of the lack of a vasculature, which then has been researched extensively[29, 30].

Materials used to construct this bio-scaffold are mostly related to the calcium phosphate family, which has similar chemical components to that of natural bone. Among the calcium phosphate family, hydroxyapatite (HA) and β-tricalcium phosphate are the main members scientists used to culture human mesenchymal stem cells.[31] The following part will briefly introduce these two calcium phosphate family members in the crystalline point of view. However, this study will not cover it all due to the short of time in master period and our experimental main focus therefore is solely narrowed on the material property of HA ceramics, specifically dissolvability.

2.3 CALCIUM PHOSPHATE

Early in 1970s, the first generation of bio-inert ceramics made of alumina was successfully implanted. Almost at the same time, interest was devoted to certain calcium phosphate phases due to their similarity to the mineral phase of bone. In 1980s, bioactive ceramics mainly

including hydroxyapatite (HA), $Ca_{10}(PO_4)_6(OH)_2$, tricalcium phosphate (TCP), $Ca_3(PO_4)_2$ and biphasic calcium phosphates (BCP, a mixture of HA and TCP) were also used in surgery.[32,33] Since then the outstanding biological properties of these calcium phosphate have been being investigated.[34,35] Based on the molar ratio of Ca/P, different names are assigned to members of the calcium phosphate family. Detailed information is listed in Table 2.1[36]. In the following sub-section, however, only HA and TCP, which are directly related to the current work, will be introduced.

Table 2.1 Calcium phosphate family.

Molar ratio (Ca/P)	Compound	Formula
0.5	Monocalcium phosphate monohydrate (MCPM)	$Ca(H_2PO_4)_2{\cdot}H_2O$
0.5	Monocalcium phosphate anhydrous (MCPA or MCP)	$Ca(H_2PO_4)_2$
1.0	Dicalcium phosphate dihydrate (DCPD), mineral brushite	$CaHPO_4{\cdot}2H_2O$
1.0	Dicalcium phosphate anhydrous (DCPA or DCP), mineral monetite	$CaHPO_4$
1.33	Octacalcium phosphate (OCP)	$Ca_8(HPO_4)_2(PO_4)_4{\cdot}5H_2O$
1.5	α-Tricalcium phosphate (α-TCP)	$\alpha\text{-}Ca_3(PO_4)_2$
1.5	β-Tricalcium phosphate (β-TCP)	$\beta\text{-}Ca_3(PO_4)_2$
1.2–2.2	Amorphous calcium phosphates (ACP)	$Ca_xH_y(PO_4)_z{\cdot}nH_2O$, n = 3–4.5, 15–20% H_2O
1.5–1.67	Calcium-deficient hydroxyapatite (CDHA or Ca-def HA)[e]	$Ca_{10-x}(HPO_4)_x(PO_4)_{6-x}(OH)_{2-x}$ $(0 < x < 1)$
1.67	Hydroxyapatite (HA, HAp or OHAp)	$Ca_{10}(PO_4)_6(OH)_2$
1.67	Fluorapatite (FA or FAp)	$Ca_{10}(PO_4)_6F_2$
1.67	Oxyapatite (OA, OAp or OXA)[f]	$Ca_{10}(PO_4)_6O$
2.0	Tetracalcium phosphate (TTCP or TetCP), mineral hilgenstockite	$Ca_4(PO_4)_2O$

2.3.1 Hydroxyapatite (HA)

The chemical formula for stoichiometric hydroxyapatite, mentioned above, is $Ca_{10}(PO_4)_6(OH)_2$ having strict Ca/P ratio of 1.67. This formula can be reduced to $Ca_5(PO_4)_3(OH)$ but $Ca_{10}(PO_4)_6(OH)_2$ is the preferred because for the two units of $Ca_5(PO_4)_3(OH)$ in the unit cell.[37] Hydroxyapatite has a hexagonal crystal structure with space group P63/m. There are 44 atoms

per unit cell and the dimensions of each unit cell are a=b=9.432Å and c=6.881Å. A model of this unit cell is shown in Figure 2.5[38].

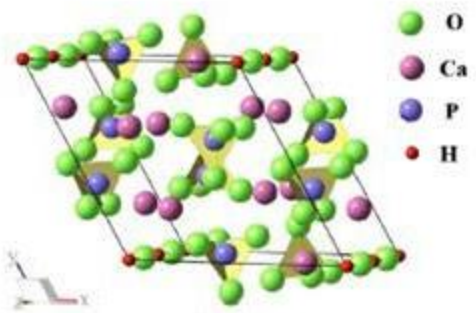

Figure 2.5 HA unit cell structure

2.3.2 Tricalcium phosphate (TCP)

Tricalcium phosphate (TCP) is polymorphic with β-TCP, α-TCP, and α′-TCP being stable as a function of temperature. Both β-TCP and α-TCP are crystalline forms of interest for biological-applications and they can both be obtained at room temperature. While β-TCP is thermally stable at lower temperatures, it will transform into α-TCP in the temperature range from 1120–1170℃.[39] The α′-TCP phase is special because it only stably exists at temperatures higher than 1430℃ and when the temperature decreases it is able to reversibly convert back to α-TCP.[40] For this reason, α′-TCP is not of practical interest compared with β-TCP and α-TCP.

Table 2.2 Structural data of α-TCP and its polymorphs

Property	$Ca_3(PO_4)_2$ polymorph		
	β-$Ca_3(PO_4)_2$ [30]	α-$Ca_3(PO_4)_2$ [28]	α′-$Ca_3(PO_4)_2$ [28]
Symmetry	Rhombohedral	Monoclinic	Hexagonal
Space group	*R3C*	$P2_1/a$	$P6_3/mmc$
a (nm)	1.04352(2)	1.2859(2)	0.53507(8)
b (nm)	1.04352(2)	2.7354(2)	0.53507(8)
c (nm)	3.74029(5)	1.5222(3)	0.7684(1)
α (°)	90	90	90
β (°)	90	126.35(1)	90
γ (°)	120	90	120
Z	21	24	1
V (nm^3)	3.5272(2)	4.31(6)	0.19052(8)
V_0 (nm^3)	0.1680(2)	0.180(6)	0.19052(8)
D_{th} ($g\,cm^{-3}$)	3.066	2.866	2.702

Figure 2.6[41] is a schematic illustration of the crystal structure of β-TCP, α- TCP, and α′-TCP along [001] projecting direction. Detailed crystal structure data of these three $Ca_3(PO_4)_2$ polymorphs are listed in Table 2.2[41]. As can be seen clearly, although they are quite similar in formula expression, considerable differences are revealed in symmetry, space group, and crystal structure parameters.

It is these considerable differences that in turn cause their different biological properties and clinical applications. While β-TCP is mainly used for making biodegradable bioceramics in the form of dense or macro-porous granules, α-TCP is mainly used in the form of a fine powder for the preparation of calcium phosphate cements. The role of both of these phases in clinical applications such as bone repair and remodeling have been studied elsewhere[34].

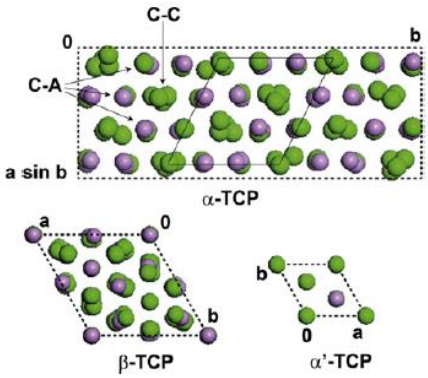

Figure 2.6 Projections of the β-TCP, α- TCP, and α′-TCP unit cells along [001] direction, where green spheres represent Ca^{2+}, magenta spheres P^{5+}, C-C are the cation-cation column, C-A the cation-anion column . O^{2-} is not shown for clarity. The solid-line rhombus outlines a cell related to that of HA.

2.3.3 Solubility of Calcium Phosphate

Solubility by definition is described as the amount of a solid that dissolves into a unit volume of solution. It is one of the most significant properties of calcium phosphates because by measuring their solubility in-vitro the in-vivo behavior can be predicted to a significant extent.[42] In the process of dissolution, calcium ions and phosphate ions are released from the ceramic into solution, and influence the cell-culturing environment. Particularly, calcium is capable of exerting influences on cells residing in the bone marrow. For example on osteoblasts[43], Shinya Nakamura and et al. reported that the morphology of cells had changed when treating them in the cell culture medium with calcium concentrations ranging from 1.8–50 mmol/L without affecting proliferation. This morphology change of cells would greatly affect Ang expression that regulates differentiation of osteogenic cells and as we all know Ang proteins is of great significance to controlling the HSCs' fate. On the plus side, HSCs are known to have Ca receptors[44], the fact of which is for sure being able to make an important influence on HSC cell

signaling[5,4]. Therefore, we need to carefully control the calcium release from synthetic calcium phosphate if these materials are to be used to mimic the HSC niche in-vitro.

Figure 2.7[45] illustrates the isothermal solubility of calcium phosphates as a function of pH values. It is not difficult to find that acid solution environment will significantly accelerate the dissolution of most calcium phosphates except mono-calcium phosphate monohydrate being equally soluble at pHs lower than 6. At pH=7~8, the common physiological condition, the range of Calcium solubility values varies from 10^{-2} to 10^{-5} M. Among these calcium phosphates showed in the graph, mono-calcium phosphate monohydrate (MCPM), $Ca(H_2PO_4)_2 \cdot H_2O$, with the Ca/P ratio of 0.5 has the largest solubility, most soluble at almost all pH values. Seen from the Figure 2.7, 1 M is reached for MCPM at pH=7, which is too high for the in-vitro culture of bone tissue. The optimal external culturing concentration of Ca^{2+} is reported to be 0.09 mM and greater concentrations would prohibit cell differentiation to a great extent.[46] At pH values from 7.35 to 7.45, which is the usual pH range for bone marrow culturing, the solubility of calcium phosphate decreases in the following sequence:

MCPM > TetCP ≈ α-TCP > DCPD > DCP > OCP >β-TCP> PHA > HA

More specifically, when checking the summary in the work of L.C. Chow and E.D. Eanes[47], Table 2.3, it is found the solubility product constants (K_{sp}) at room temperature of β-TCP, α-TCP, HA , and TetCP are $10^{-28.9}$ M, $10^{-25.5}$ M, $10^{-58.4}$ M, and $10^{-38.0}$ M respectively. And K_{sp} of $CaCO_3$ is $3.3*10^{-9}$ M. These magnitude differences suggest $CaCO_3$ be much soluble than α-TCP, β-TCP, TetCP, and HA, among which HA is the most insoluble one.

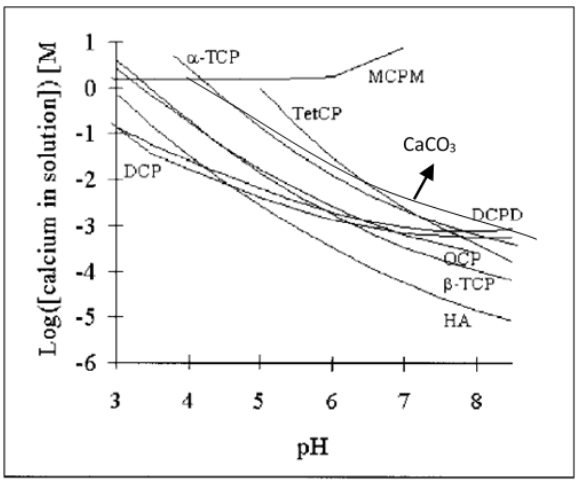

Figure 2.7 The concentration of Ca as a function of pH from dissolution of MCPM, mono-calcium phosphate monohydrate; Tetracalcium phosphate (TetCP); Dicalcium phosphate dehydrate (DCPD); Dicalcium phosphate (DCP); Octocalcium phosphate (OCP)

As one of the main objectives in this study, dissolution of HA in water can be expressed as an equilibrium of ions (Ca^{2+}, PO_4^{3-}, HPO_4^{2-}, HPO_4^{2-}, H_2PO^{4-}, H_3PO_4, and OH^-):

$(n_c\text{-}1)H_2O + Ca_5(PO_4)_3(OH) \rightarrow 5\ Ca^{2+} + 3x_1PO_4^{3-} + 3x_2HPO_4^{2-} + 3x_2H_2PO^{4-} + 3x_4H_3PO_4 + n_cOH^-$, where n_c represents the mole number of protons consumed when 1mol HA is dissolved, x_i (i=1~4) the mole fractions of the different phosphate forms present in the solution.

Table 2.3 Calcium phosphate compounds and their solubility constant

Compound	Formula	Ca/P	–log (Ksp) at 25 °C
Monocalcium phosphate monohydrate	$Ca(H_2PO_4)_2 \cdot H_2O$	0.5	highly soluble
Monocalcium phosphate anhydrous	$Ca(H_2PO_4)_2$	0.5	highly soluble
Dicalcium phosphate anhydrous	$CaHPO_4$	1.0	6.90 [McDowell et al., 1968]
Dicalcium phosphate dihydrate	$CaHPO_4 \cdot 2H_2O$	1.0	6.59 [Gregory et al., 1970]
Octacalcium phosphate	$Ca_8H_2(PO_4)_6 \cdot 5H_2O$	1.33	96.6 [Tung et al., 1988]
α-Tricalcium phosphate	$\alpha\text{-}Ca_3(PO_4)_2$	1.5	25.5 [Fowler and Kuroda, 1986]
β-Tricalcium phosphate	$\beta\text{-}Ca_3(PO_4)_2$	1.5	28.9 [Gregory et al., 1974]
Hydroxyapatite	$Ca_5(PO_4)_3OH$	1.67	58.4 [McDowell et al., 1977]
Fluorapatite	$Ca_5(PO_4)_3F$	1.67	60.5 [Moreno et al., 1977]
Tetracalcium phosphate	$Ca_4(PO_4)_2O$	2.0	38.0 [Matsuya et al., 1996]

2.4 SINTERING

In this section, we will discuss sintering in general and then specifically the sintering of HA.

2.4.1 General sintering

Sintering is a crucial thermal treatment for the fabrication of ceramics, the process bonds ceramic particles into a coherent and solid structure by mass transport on the atomic scale and leads to the evolution of the final microstructure. This thermally induced bonding leads to lowering the system free energy, the global driving force for the process. The temperature used to sinter is much lower than the melting temperature during solid state sintering. Microstructurally, sintering is a complex process involving radical changes in the number of grains, grain size, grain shape, surface area, and pore population and often controls the final properties of the ceramic.[48]

Density is the common descriptor of the sintering process and is commonly used to study sintering kinetics. There are at least three different definitions of density for a porous ceramic and their comparison can be used to gain extra information about sintering microstructures such as the fraction of open and closed pores through the sintering process. Theoretical density refers to the pore-free solid density while true density, apparent density, and bulk density are used to characterize porous materials.

1) True density is defined by mass/volume without pores and therefore equals the theoretical density. To measure the true density the sample is weighed in air getting mass m_1. Second, the sample is weighed suspended in water to obtain its mass m_2. Then true density is calculated by

$$\rho_{TD} = \rho_{fluid} \frac{m_1}{m_1 - m_2}$$

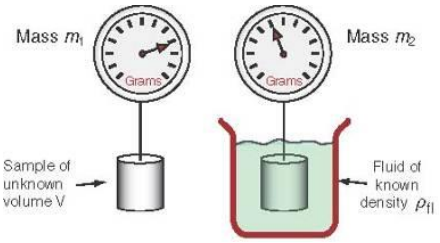

Figure 2.8 Measurement of true density

2) Then apparent density equals

$$\rho_{AD} = \rho_{fluid} \frac{m_1}{m_1 - m_2}$$

This will be different from the true density if the sample contains closed pores

3) The bulk density takes into account open pores, closed pores, and solid and is calculated using

$$\rho_{BD} = \rho_{fluid} \frac{m_1}{m_3 - m_2}$$

, where M_3 is weight of the sample in air with all the open pores filled with water.

In addition, the bulk density of the un-sintered material is called the green density

Lots of studies[49,50,51,52,53,54] have been conducted on sintering and the theory is well established. While sintering microstructures are quite complex it is common practice to treat microstructural evolution in sintering in terms of three idealized stages that are easily modeled as illustrated in Figure 2.9[47].

In the initial sintering stage, necks form connecting neighboring particle and these contacts will enlarge without interaction with neighboring contacts. Necks grow via short-range

motion of atoms. Most of the particles will be misoriented so, grain boundaries form at the necks. Figure 2.10[42] is a SEM image showing the neck growth during the sintering of nickel particles. As the necks grow by densification mechanisms such as volume diffusion or grain boundary diffusion, the centers of these contacting particles will approach each other resulting in macroscopic shrinkage of the sample. If the necks grow by surface diffusion or evaporation-condensation mechanisms, the centers of the particles do not approach one another and there is a loss of surface area without macroscopic shrinkage. The density in initial stage sintering is limited to about 65% of the relative density due to the overlap of adjacent necks, which means there is still 35% of volume that is occupied by pores.[55] To quantitate sintering stages, neck diameter X and the particle diameter D are defined as sketched in Figure 2.11[42]. With regard to the initial stage, values of X/D are less than or equal to 0.33 and the pore structure is open allowing gas to permeate through the sintering microstructure. Hence the true density and apparent density should have the same value and the bulk density value will be much lower.

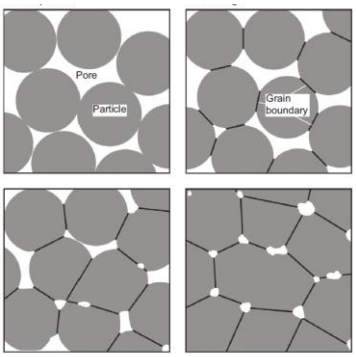

Figure 2.9 Three Idealized stages of general sintering

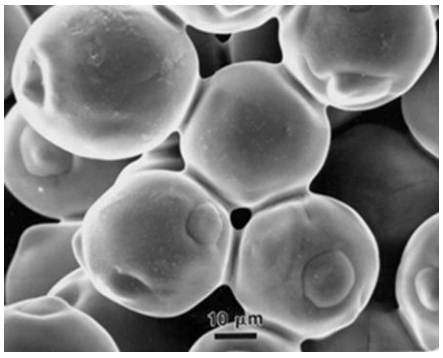

Figure 2.10 SEM image of neck growth

In the intermediate stage of sintering, the necks continue to grow and overlap. The grain boundary area in the neck also enlarges while neighboring necks impinge on to create grain

edges. The grains have polygonal shapes with planar facets while the pores are represented by connected cylinders along the grain edges. Generally, the value of X/D (neck size ratio) locates in the range from 0.33 to 0.50. Additionally, it is in the intermediate sintering stage that shrinkage and sintering rate peak. Since the pores remain fully connected the apparent density will have the same value as the true density and the bulk density will have a lower value. The grains can begin to grow in this stage of sintering.

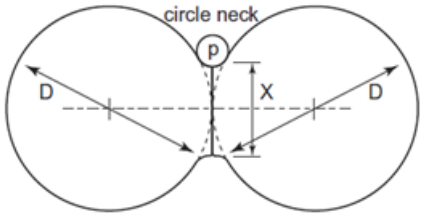

Figure 2.11 Illustration of neck growth

The transition from a microstructure composed of a continuous pore network along the edges of grains to polyhedral grains and isolated pores at grain corners representing the beginning of final sintering stage. This transition can be detected because the onset of pore closure will reduce the apparent density to values below the true density and the apparent density and the bulk density will have the same value when all the pores are closed. When all the pores are removed then only the true density can be defined. Generally, this transition from intermediate to final stage sintering occurs at the relative bulk densities ranging from 90% to 92%. An idealized final stage microstructure can be represented using tetrakaidecahedronal grains showed in Figure 2.12[42], which has 12 faces, 30 edges, and 24 corners. Importantly, the pores in final stage sintering are thought to be pinned at the grain corners, each of them is shared with four grains giving six pores per grain if all the grain corners have pores.

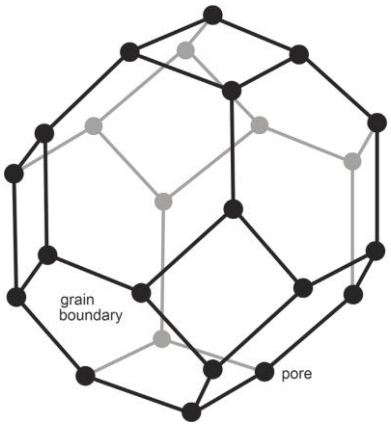

Figure 2.12 Ideal grain shape in final stage sintering

Experimental measurements indicates that closed pores can be detected in real microstructures at 85% density, approximately half are closed at 92% density, and almost all pores are closed at 95% density. The distinction between the microstructural properties for the three stages are listed in Table 2.4[42].

Table 2.4 General properties summarized for three sintering stages

	Initial Stage	Intermediate Stage	Final Stage
neck size ratio, X/D	<0.33	0.33 to 0.5	>0.5
coordination, N_C	<7	8 to 12	12 to 14
density, %	60 to 66	66 to 92	>92
shrinkage, $\Delta L/L_O$ %	<3	3 to 13	>13
surface area, S/S_O %	100 to 50	50 to 10	<10
grain size ratio, G/D	≈ 1	>1	$>>1$
pore size ratio, d/G	<0.2	near constant	shrinking

X = neck diameter, D = particle diameter, N_C = coordination number.
$\Delta L/L_O$ = sintering dimensional change over initial size, commonly termed shrinkage.
S = specific surface area, S_O = initial specific surface area prior to sintering.
G = grain size, G_O = starting grain size, d = pore diameter.

It is knowing the general stages of sintering that incites researchers thinking that how we control these stages so that a better or as-wished property of the sample could be tailored? This brings us to the kinetics of sintering. In the following section, hydroxyapatite ceramics, the main role of this work, will be taken for an example to detail how experimental parameters, such as sintering temperature and time etc., exert influences on sintering kinetics.

2.4.2 Sintering of Hydroxyapatite (HA)

Dense HA bodies having the relative density higher than 95% with fine microstructure can be obtained by sintering, the temperature of which is typically higher than 1100℃. However, this doesn't mean that sintering temperature can be increased unlimitedly in order to get fully densed HA ceramics. It is often being limited by the decomposition of hydroxyapatite.[56]

Sintering temperature is crucial in the densification of HA. The temperature of initial decomposition, HA → 2TCP + TetCP + H_2O (TetCP refers to tetracalcium phosphate), varies: 1050℃[57], 1300℃[58,59], 1400℃[60] or even 1477℃[61]. These differences could be attributed to the purity of HA, the nature of HA, and the environmental conditions, such as humidity. Among these factors, water vapor plays a role of great importance. Results from P.E. Wang and T.K. Chaki[62] found that decomposition temperature increased up to 1350℃ when HA samples were sintered in moisture atmosphere. This makes sense as we look into the initial decomposition that HA is decomposed to release H_2O. While the atmosphere is filled with water the reaction that leads to the right direction is inhibited and as a result the decomposition of HA is delayed. Researchers have also found that different synthetic paths of hydroxyapatite make a discrepancy in sintering behavior[63].

Cihlář, J. and et al.[64] studied the kinetics of thermal decomposition of HA and classified the decomposition procedure of HA into four steps, which are sintering, removal of water, decomposition of HA to TCP, and formation of TetCP. X-ray results revealed that:

1) From 900 - 1350℃, $2Ca_5(PO_4)_2OH \rightarrow Ca_{10}(PO_4)_6Ox(OH)_2(1-x) + xH_2O$, where $0 \leq x \leq 1$;

2) From 1350 - 1458℃, $Ca_{10}(PO_4)_6O_x(OH)_2(1-x) \rightarrow 3Ca_3(PO_4)_2 + CaO + (1-x)H_2O$;

3) Above 1477℃ TetCP started to form, $Ca_3(PO_4)_2 + CaO \rightarrow Ca_4(PO_4)_2O$.

This was supported by the fact that TCP was first identified on sintered surfaces after sintering at 1350℃. The decomposition occurs at 1350℃ and above would have detrimental effects on the sintered density.

Regarding the present study, we choose 1100℃ to firstly pre-sinter the pressed green pellet giving the sample some strength but not allowing the density to increase so much that the pores begin to close. The inter-connected pore structure is require for the study so that a second phase can get impregnated into the partially sintered material. Then for the sintering temperature was increased 1300℃ to allow final stage sintering to be achieved without any decomposition of HA to TCP.

2.5 INFILTRATION OF POROUS CERAMICS WITH SECOND PHASE PRECURSORS

Porous material with connected pore channels can be infiltrated with the second phase by immersing the material in a solution that has the required chemical precursors. After enough infiltration time, pore channels will be filled with the precursor solution by capillary action of a

wetting liquid. Then drying followed by the decomposition of the chemical precursors, crystallization of the second phase and sintering can be used to introduce a second phase. However, due to the evaporation of the solvent from the external surfaces during drying the precursor will preferentially exceed its solubility and precipitate in the pore structure at or near the surface from which evaporation is taking place. Therefore one would expect a gradient of the second phase in the ceramic with highest concentrations at the surface and lower concentrations in the interior. These gradients of second phase have been detected in infiltrated and sintered ceramics.[65,66]

The infiltration process has been adopted to create functionally graded materials.[52,67,68] Infiltration depth can be controlled both by infiltration time or the concentration of the precursor in the solution. With this control, compositionally grading material can be explored for a range of applications.[60,61]

Infiltration technique has been employed to make multiphase ceramics. An alumina/mullite ceramic was prepared by infiltrating porous alumina with a SiO_2-containing sol by Marple and Green[52]. They found that the mullite content decreased gradually from the sample surface to the interior and the alumina grain size tended to increase with the distance from the sample surface, perhaps due to grain growth control by the second phase. Honeyman-Colvin and Lange[69] prepared an alumina-based material infiltrated with tetragonal $Zr(4Y)O_2$ and a high mean strength of 588 MPa is obtained. The reason for its strength high strength was that the grade layer created compressive residual stress on the sintered surface. Infiltration is also considered to be a significant processing route to form composites using macroporous structure.[70] In the study of HA scaffolds, Shahriar Sharifi and et al.[71] reported that polymer infiltration could improve the compressive strength of HA scaffolds up to 14 – 328% depending on what type of the polymer

(PCLF or PCLI) and the concentration of are used. All of these studies show that infiltration can be used to tailor the composition and microstructure of ceramics.

3.0 HYPOTHESIS

High calcium is known to promote HSC expansion and cell growth. Indeed biphasic HA-CaO ceramic scaffolds have been used to enhance the release of calcium ions into HSC culture medium and thereby control HSC fate while still remaining biocompatible.

Therefore the hypothesis of this MS thesis is that precursor concentration used in infiltration can be used to control the gradient of CaO close to the external surface of biphasic HA-CaO ceramics and thereby control the time-dependent release of calcium ions into saline. The extra CaO incorporated into the sample will transform to $CaCO_3$ causing the volume change, which will result in fragmentation of the material. Then an enhanced degradability of the material can be expected. Apart from making cacium-rich HA by infiltration, mixing CaO with HA powder is also conducted in this study to make a comparison with the infiltrated one.

4.0 OBJECTIVES

1. Partially sintered HA ceramics will be infiltrated with calcium nitrate precursors to produce CaO second phase in-situ after full sintering. Similar HA-CaO ceramics will be processed by mixing HA powder with calcium nitrate prior to calcination, pressing prior to sintering. The effect of molar ratio of Ca/P on CaO/$CaCO_3$ phase fraction, weight changes and damage area fraction will be studied.

2. Time points of 0.5 hour, 1 hour, 1 day, 3 days, 1 week, 2 weeks, 4 weeks are determined to study the weight changes and the microscopic morphologies after the solubility test both of the infiltrated ceramics and of ceramics made by mixing.

5.0 APPROACH

As far as the approach we adopt to prepare, test, and characterize our samples, detailed information will presented below. All raw materials and instruments we use are listed in Table 5.1.

Table 5.1 Experimental materials and instruments list

Category	Model or provider
Hydroxyapatite powder	Sigma–Aldrich
Calcium nitrate tetra-hydrate	$Ca(NO_3)_2 \cdot 4H_2O$, Alfa Aesar, England
Saline	Tris Buffered Saline (TBS), pH=7.4
Purify & Calcine furnace	Thero Electron Corporation, Lindberg/Blue M
Sintering furnace	Lindberg/Blue M, Kendro Laboratory Products, Inc.
Magnetic stirrer	Corning Stirrer/Hot Plate (PC-320)
Drying oven	Isotemp Vacuum Oven (282A), Fisher Scientific
Press	Carver Laboratory Press (36000-223)
Polishing machine	Grinder-polisher, Buehler
SEM	JOEL SM6610LV
XRD	Empyrean, The Analytical X-ray Company

5.1 SPECIMEN PREPARATION

Experiment of this work begins with calcination of commercial HA powder at 900℃[72] for 1h. Afterwards, calcined HA powder was ball-milled for 24h and then put into the oven for complete drying. Finally, a pestle and mortar was used to granulate dried powder. Hereto, the pre-processing of HA powder is complete.

To ensure every sample has the same dimension, granulated HA powder was weighed on the balance giving each sample 1g in mass. Evenly weighed HA powders were pressed using a metal mould with 13mm in diameter into pellets, which then were followed by partial-sintering at 1100℃ and full-sintering at 1300℃. Pressure applied for making the pellet is controlled, which is 26 MPa. Both of these two sinterings have heating rate and cooling rate of 5K/min and 10K/min, respectively. Results from experimental measure indicates that the green density of samples right after pressing averages around 49.5% and the density after pre-sintering is around 67%. Preparation procedures described hereto are the process of making control samples that are not treated with infiltration and are composed of sole pure HA powder. Procedures of infiltrated and mixed specimens vary in certain above-mentioned steps.

In case of infiltration sets, pellets after partial sintering were infiltrated in the solution of calcium nitrate tetrahydrate. Calcium ions of 5 mole per liter are determined to do the infiltration process. Firstly, after finishing preparing the calcium nitrate solution samples prior to full sintering are immersed into this Ca^{2+} concentrated solution for 24 hours in the vacuum container. Secondly, infiltrated samples are taken out from the beaker and immersed again but this time in ammonia solution with pH ranging from 12 to 13 for 0.5 hour in order to stabilize the Ca^{2+}. Thirdly, samples were taken out from the ammonia solution and air-dried in the fume hood for

24h. There is one more step to go before full sintering, which is the calcination at 900℃ again with the purpose of transforming the calcium-containing phase into crystallized CaO. Samples undergo the above process are denoted as 5MHA in a convenient manner.

While in case of mixing, ground HA powder was slowly added into calcium-nitrate-dissolved solution, the concentration of which was determined based on the weight percentage of $CaCO_3$ that would exist in pellet after calcination at 900℃. In this work, 5wt% and 10wt% of $CaCO_3$ are concerned. In case any disintegration would occur in the process, solvent used here was ethanol, which also gives less surface tension under drying. Upon the adding of HA powder, the solution was magnetically stirred for better blending. The stirring process continues for 0.5h and after that the beaker was put under the heat lamp to have a complete dry. Mixed powder then was ground again and calcined under the identical calcining condition before making mixed pellets.

Due to consideration that our specimens are in large quantity and great amount of time will be consumed in polishing, sixteen samples, four pellets in each category, are chosen to do one-side polishing. Polish work begins with impregnating samples into a viscous resin and until the resin becomes hard enough immobilizing the sample, this transparent yellow resin mould will be held by a holder to get machine-polished with diamond pastes in different microns in the following sequence: 45μm, 30μm, 15μm, 6μm, and 1μm. Surface study will also be done on these polished samples assisted by SEM at four representative time points, which are 1 hour, 3 days, 1 week, and 4 weeks.

Regarding the densification aspect, studying the densities of samples after different sintering times is also the work of interest. To do so, different sintering times, 0.5 hour, 1 hour, 2 hours, and 5 hours, are carried out.

Interestingly, samples after sintering revealed obvious discrepancies in color, dimension, and density. While pure HA and infiltrated one display blue in color, 5wt% and 10wt% mixed samples show light blue and white respectively.

In a convenient manner, abbreviations are applied which are listed in Table 5.2.

Table 5.2 Abbreviations of each category

Category	Abbreviation
Pure HA	HA
infiltrated HA by 5M calcium nitrate solution	5MHA
5wt% mixed HA	5WTHA
10wt% mixed HA	10WTHA

5.2 SOLUBILITY TEST

Sintered specimens are weighed and measured in dimension for record before being immersed into saline (Tris-buffer Saline). Then a change in mass can be observes after the saline treatment. Each pellet was soaked in saline in a sealable tube and held on a holder for each corresponding time. Each tube has 50 mL saline in volume. Soaked samples were tweezed out from saline and air-dried in the hood when the time point has been met. When they are completely dried in the hood, masses of them are weighed individually again.

5.3 CHARACTERIZATION

Since surface conditions are the main work of this research, it is necessary for us to get the surface components and microscopic pictures of samples. Only having these information better understandings and analyses of their behaviors can be obtained and conducted. With this being said, it is the XRD and SEM that we have chosen to characterize our samples. Samples both before solubility treatment and after 4-week exposure to saline are x-rayed to reveal the phase condition on surface. SEM work is done on polished samples in order to give a better contrast in image. Doing so etching effect will be more obvious to see without the distraction of unpolished rough surface. Each pellet will be coated with palladium first before scanning. In addition, EDS (element analysis) will be involved when necessary.

6.0 RESULTS AND DISCUSSIONS

In this section, we will present the results on sintering and the weight change, phase transformation and surface damage caused by the dissolution of the calcium rich phases along with the explanations of the behavior.

6.1 EFFECT OF SINTERING TIME ON RELATIVE BULK DENSITY

Figure 6.1 is the relative bulk densities of all the samples as a function of increasing sintering time from 0.5 hour to 5 hours at a temperature of 1300℃. In general, taking into consideration the error bars, the density of the samples made by mixing increase with sintering time. For 10wt% $CaCO_3$ mixed samples, the effect of increasing sintering time is distinct: when the sintering time is increased from 1 to 2 hours, the density increased from 82% to 87%. Relative densities of 5wt% and 10wt% groups eventually reached 94% and 87%, respectively after 5 hours. For the 10wt% samples, it is believed the density never reaches 90% and so it is thought there are still open pores inside the pellet, as commonly observed in sintered materials. However, there is no significant difference in density at any of the sintering times for pure HA and 5M infiltrated samples. Densities of these two sets are all above 95%, at which point it would be expected that the remaining pores will be closed.

Hence, it is concluded that: increasing sintering time is able to increase the density of the mixed samples, particularly for the 10wt% mixture. However increasing the sintering time leads to no further increase in the density of the HA and the infiltrated samples, which are significantly denser than those made as mixtures. The pores in the 10wt% mixed samples are expected to be open but those in the HA and the infiltrated materials are expected to be closed.

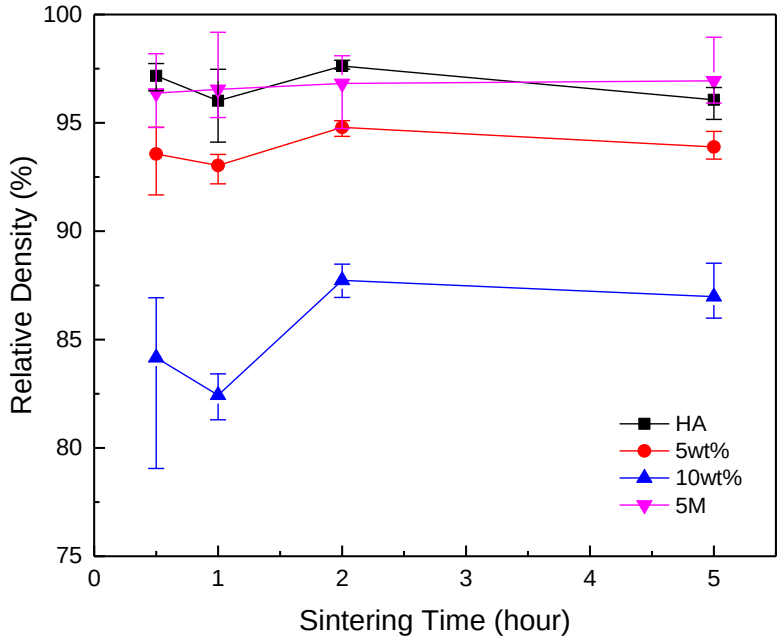

Figure 6.1 Effect of sintering time on relative density of samples.

6.2 XRD RESULTS

For HA, there are two important types of impurities mentioned in the literature that can affect phase stability[73]. One is elements such as Mg, C, F, and etc., the other is CaO or non-stoichiometric HA, which are composed of Ca, P, O and H but have a Ca/P ratio different from

1.67. In our study, the latter one is the situation. The HA powder used in this study had lower Ca/P, which revealed by EDS is around 1.60.

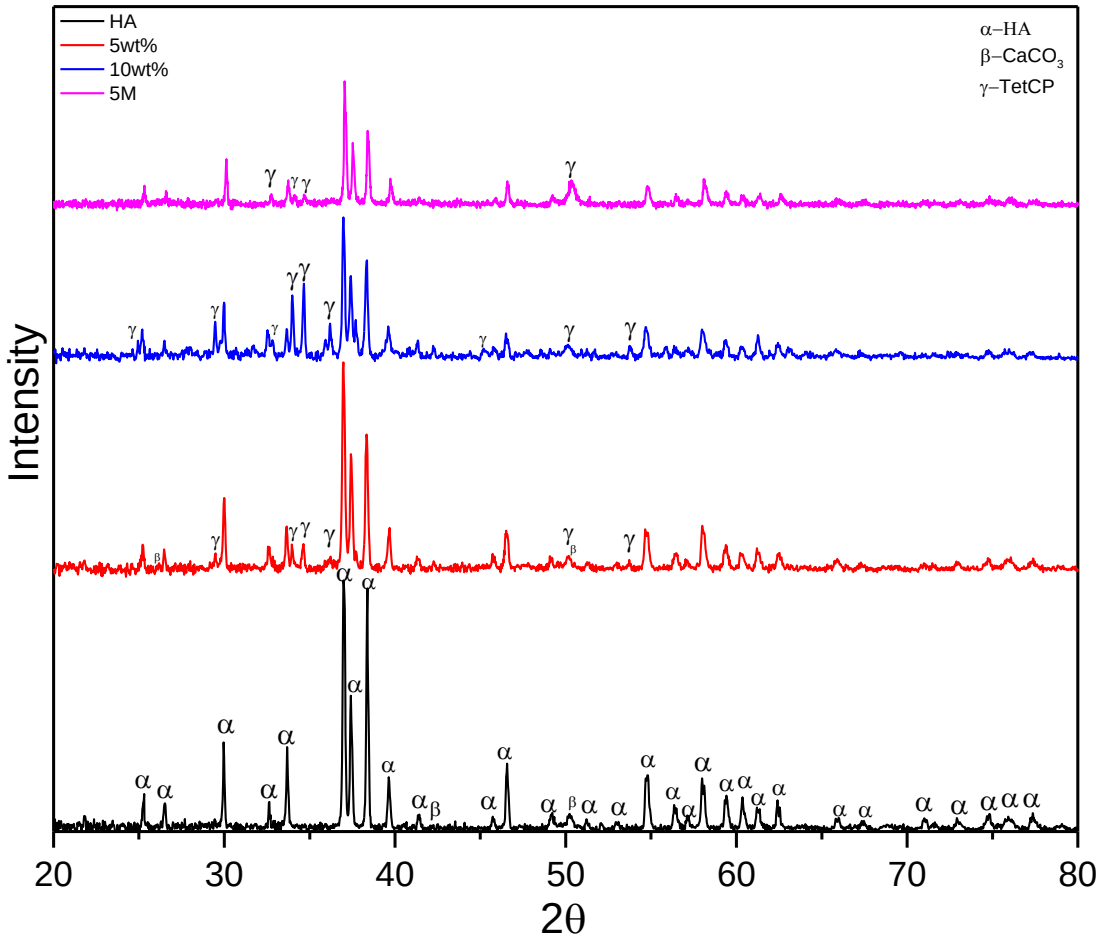

(a) Before solubility test

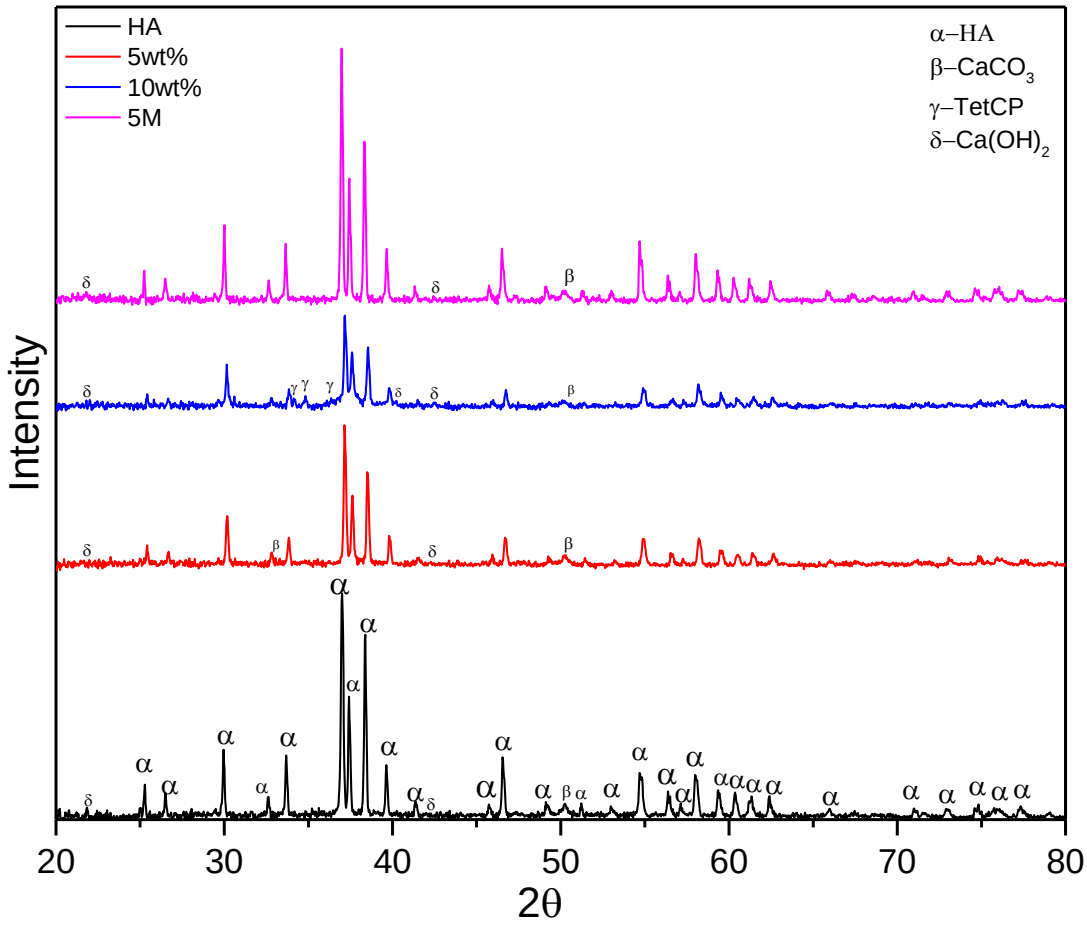

(b) After 4-week exposure to TBS

Figure 6.2 Diffraction peaks of samples (a) before solubility test, (b) after 4-week exposure to TBS

Figure 6.2 presents the diffraction peaks of detected phases in our samples both before solubility test and after 4-week exposure to TBS. For convenience and clear demonstration, HA phase is marked as α while $CaCO_3$, $Ca(OH)_2$, and TetCP as β, δ, and γ respectively. All distinct HA peaks are labeled in HA set (black lines in Figure 6.2) while only impurity peaks are denoted in other three categories. According to the XRD results in Figure 6.2a, regarding the pure HA sample there is small peak located at slightly higher angle than $2\theta = 50°$ (denoted as β in the figure) suggesting the existence of calcium carbonate phase, which is a result of the reaction

between exposed CaO on the surface and CO_2 in ambient air. Calcium oxide is the phase that theoretically should not exist in our sample particularly that the powder is calcium deficient HA. It may be that a small amount of the HA may have decomposed to TCP and CaO as described in section 2.4.2. However, we did not detect distinct peaks of TCP. Perhaps its fraction is just too small to be detected. This suggests that the HA samples are not entirely phase pure and CaO on the surface has formed 6wt% calcium carbonate on exposure to a moist environment as shown in Figure 6.3a.

Phases detected on our samples before solubility test are compared in Figure 6.3a. They are: hydroxyapatite, calcium carbonate, and tetracalcium phosphate (TetCP). The peaks associated with TetCP are somewhat broad. Since the mixed samples incorporated 5wt% and 10wt% equivalent $CaCO_3$ into HA, the ideal molar ratios of CaO/P_2O_5 in the samples are 77.83% and 78.75% respectively. Based on these two values, their compositions are located in the equilibrium C_4P and C_3P two phase field for un-hydrated calcium phosphate as shown in red circled area in phase diagram, Figure 6.4. Hence, the occurrence of TetCP is not surprising but the phase fractions were high, especially for the mixed samples. There was no calcium hydroxide detected in the samples before treatment. The amount of TetCP both in mixed and infiltrated samples is significant, especially in the 10wt% mixed specimens where the percentage of TetCP is as high as 57% and even dominates over HA main phase. It is also interesting to find that calcium carbonate, is not present only in the 10wt% sample.

Figure 6.3b gives the phase distribution on the surfaces of the samples after 4-week soaking in TBS. Small amounts of calcium hydroxide was now present after immersion on all of the samples. After the solubility test, TetCP is absent on the surface of the 5wt% mixed samples and 5M infiltrated samples and there is a large decrease in the amount of TetCP on the surface of

the 10wt% mixed sample. The decrease of the TetCP on the surface of the sample is consistent with dissolution in the saline since the solubility of this phase is so high, Figure 2.7.

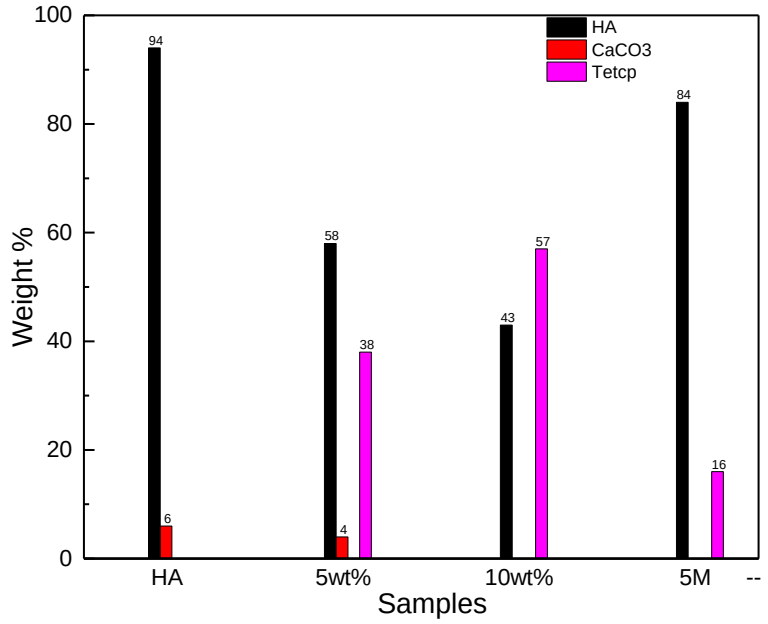

(a) Before solubility test

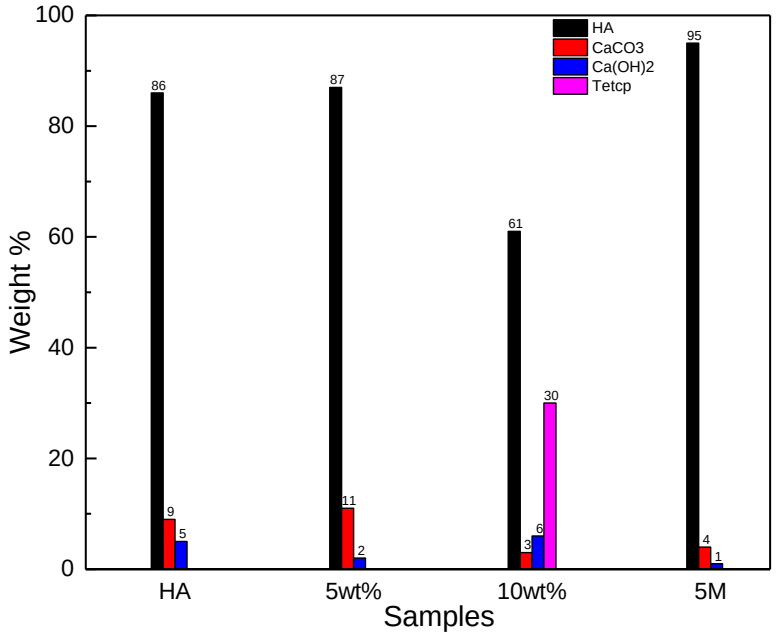

(b) After 4-week exposure to TBS

Figure 6.3 Weight percentage of the components in samples

Therefore, it is concluded that extra CaO incorporated into the samples no matter by mixing or by infiltration causes the formation of TetCP; and after 4-week solubility test, small amounts calcium hydroxide was seen in all samples; but large decreases in the amount of TetCP are observed, probably due to dissolution in the saline.

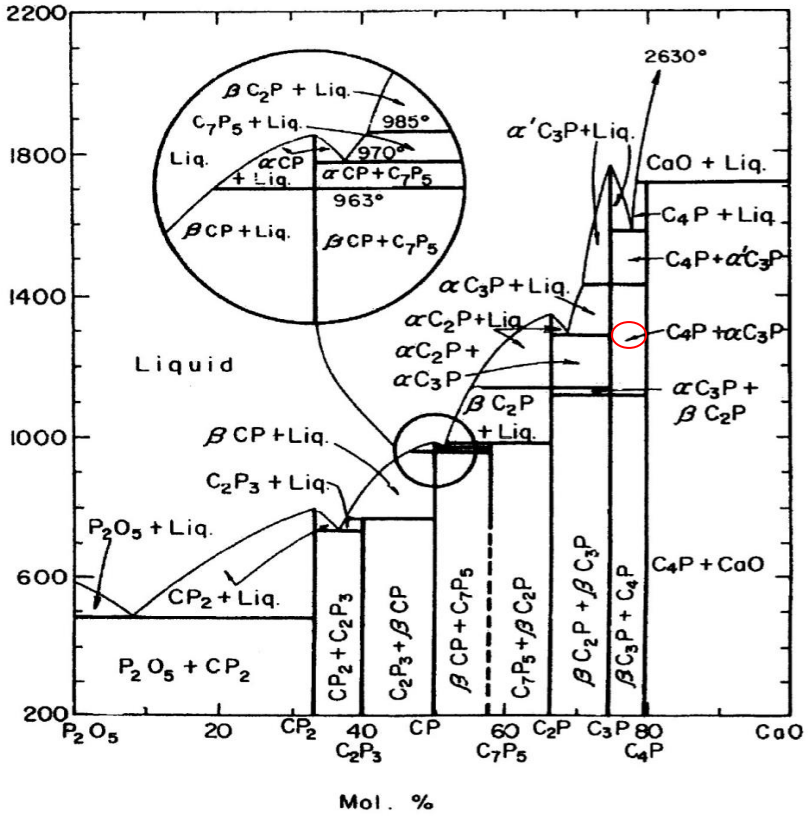

Figure 6.4 Phase diagram of CaO and P_2O_5 in mole %[74]

6.3 WEIGHT CHANGE AFTER THE SOLUBILITY TEST

Figure 6.5 gives the weight change in percentage based on the original mass that had been determined before solubility test. In the graph, 0.00 (Zero) marks no difference in weight

occurred after the solubility test, and all values under this offset represent a mass loss after immersion in TBS while values above this line represent a mass gain. It is clear that the weight changes are very small, less than 1%, even after 4 weeks so the error bars are relatively large for some conditions and this can affect the interpretation.

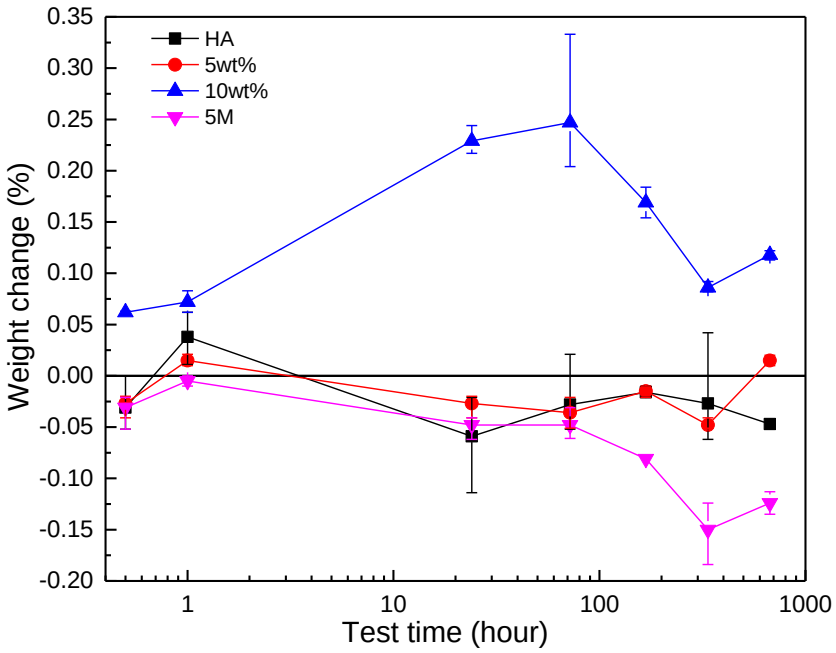

Figure 6.5 Weight change in percentage of all samples at all time points

It is clear that samples in the 10WTHA group show relatively large weight gain in the first three days of immersion but after 3 days the weight gain decreases once more and then stabilizes after 2 weeks. Specimens of 5MHA group seem to consistently lose weight, especially after 3 days then it appears to stabilize after 2 weeks. For the weight of the HA and 5WTHA specimens both seem to fluctuate around zero but most imply a small mass loss.

The increase in weight for the 10WTHA is most likely due to the precipitation of amorphous calcium phosphate phases early in the soak period caused by the release of calcium

and phosphate ions from the material as the TetCP dissolves[81], this exceeds the solubility of the amorphous calcium phosphate phase in the saline, the net gain in weight being due to the incorporation of oxygen, hydrogen and carbon from the saline. It is interesting that there is a small gain in weight at 1 hour and may be due to the same precipitation on all samples. While the weight gain continues over a 3 day period for 10WTHA the other conditions seem to show mass loss after the first hour, especially the 5M infiltrated sample. Interestingly the mass loss seems to stabilize after 2 weeks for the 10WTHA and 5M infiltrated samples.

Thus, we may conclude: some precipitates may have already formed after 1-hour exposure to TBS in all cases; 10wt% mixed samples clearly gains weight in the first 3 days of immersion but this tendency slows down after that and the material begins to lose weight. The 5MHA samples, show a continuous mass loss especially after 3 days. Then the mass loss stabilizes after 2 weeks. No clear trend is seen in the pure HA and the 5WTHA but most conditions show a small mass loss.

6.4 MICROSORPIC IMAGING

Summarized from other accessible literatures, several factors have been proposed to play significant roles in the degradation of HA:

1) Physical characteristics, including HA form (foam or bulk), porosity, and grain size.[75,76]
2) Stoichiometry (Ca/P ratio), calcium phosphates that rigidly stick to the Ca/P ratio of 1.67 have the lowest rates of degradation compared to any other calcium to phosphorous ratios.[77]
3) Impurity ions, like CO_3^{2-} can create carbonated HA[78], while F^- ions create fluorapatite[79]. The former exhibits higher degradation rate while the latter lower degradation rates.

These factors should be kept in mind when evaluating the microscopic evidence of degradation in this study.

6.4.1 HA

It can be seen from Figure 6.6a and b that the polished sample surface maintains its polished condition with some polishing scratches visible after 1 hour in saline. The surfaces were not significantly different from the as polished condition. Damage created by dissolution are observed on surfaces exposed to saline for longer times. Figure 6.6c and d, shows a sparse population of damage clusters after 3 days which have obvious facets probably associated with grain removal that could contribute to a small amount of mass loss. These defects were not observed after 1 hour.

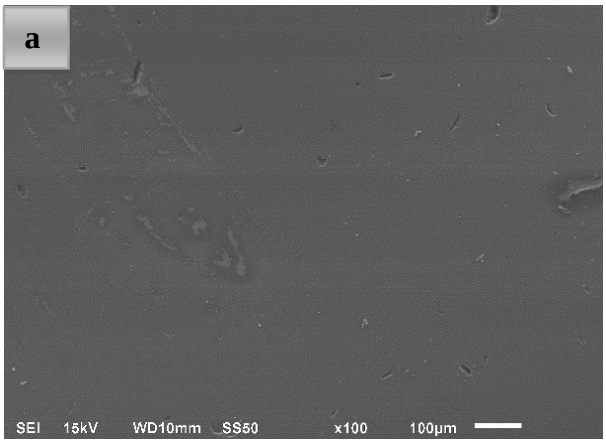

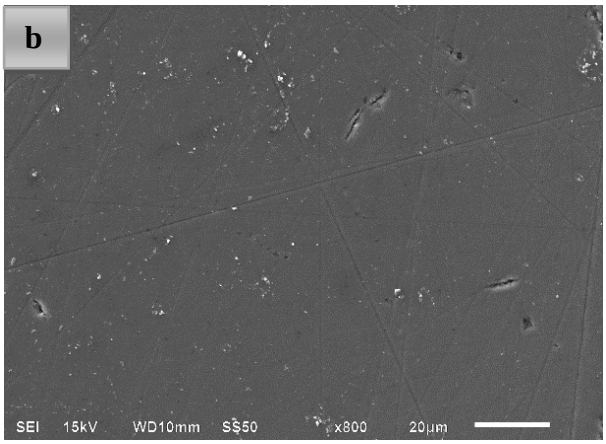

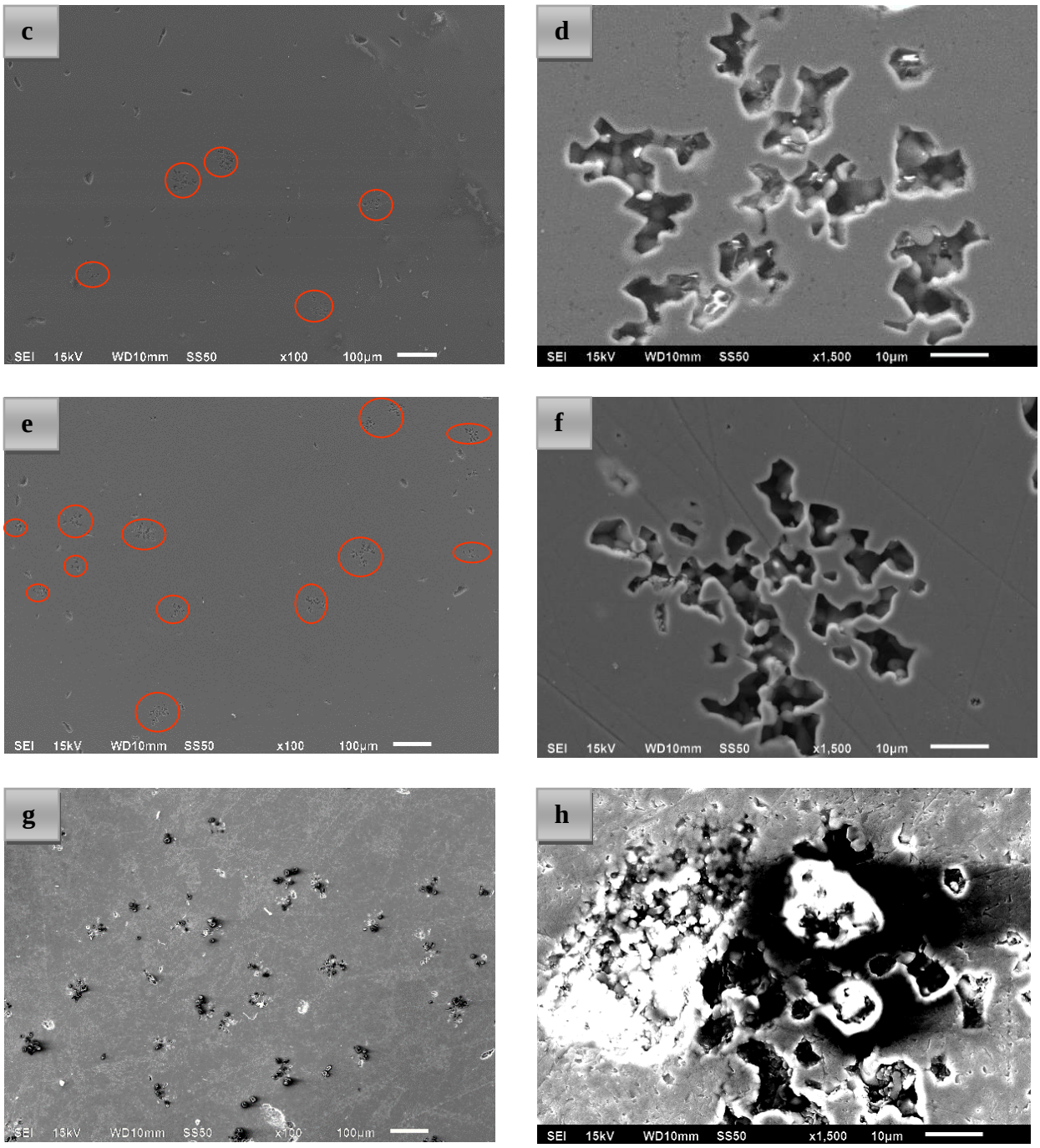

Figure 6.6 SEM images of HA after the solubility test, where a, c, e, g represent 1-hour, 3-day, 1-week, 4-week figures respectively in low magnification, and b, d, f, h are corresponding figures in large magnification.

The damages created by saline appeared as small clusters holes that have grain shape. According to Haibo Wang[80], angular shape damages indicate the presence of CaO. Yet the

number of these damages is still in low amount and an area fraction of only s 0.20%. In the interior of the damage, the grains underneath the surface can be observed. Therefore the minor mass losses in HA could be associated with the removal of grains Figure 6.8(a) shows that the area fraction of damages increased with immersion time with fractions of 0.90% and 1.16% are obtained after 1 week and 4 weeks respectively. Surface precipitation does not seem to be a factor in the degradation of the pure HA.

The depth of the damages appears to increase with increasing soaking time as darker area is displayed in Figure 6.6f. Figure 6.8a shows that there is a general increase in the area fraction of the damage over 4 weeks and this correlates inversely with weight loss as one would expect.

The depth of damages cannot be clearly seen in the 4 week sample since precipitates gather in the hole as can be seen in Figure 6.6h. Based on this observation it is logical to infer that locally different physi-chemical environments may exist, where precipitates area preferentially seen. Hence the solubility limit for the precipitating phase may be exceeded near the damage sites.

Therefore, to conclude the HA samples show a sparse population of damage that increases with increasing soak time and seems to correlate inversely with the weight loss of the sample. The damages have a faceted shape, and tend to form clusters. This could be consistent with a non-uniform spatial distribution of a small amount of calcium oxide in the sintered sample that creates damage, possibly removing adjacent HA grains when it transforms to $CaCO_3$ on exposure to air and saline. This would result in damage and the detection of $CaCO_3$ on the surface of the samples by XRD. Interestingly the amount of $CaCO_3$ detected on the surface increased slightly after 4 weeks of exposure and there is a detectable increase in the amount of damage on the surface.

6.4.2 5MHA

Damages in the surface is 5M1h are obviously much more severe than that in HA material even 1-hour exposure to TBS is enough to create a damage area fraction of 23.4% on the surface of the sample. Recalling the XRD results the 5MHA sample the surface before exposure to saline contained HA and significant amounts of TetCP and $CaCO_3$ which are both highly soluble. TetCP, has the largest Ca/P mole ratio of any calcium phosphates, up to 2, and has a much higher dissolution rate than HA and TCP.[81] The dissolvability of the phases of interest goes in sequence: HA<β-TCP<α-TCP<TetCP<$CaCO_3$, which can be obtained from Figure 2.7. Taking this into consideration, the fast appearance of damage on the surface of 5MHA is to be expected. Again CaO incorporated into the ceramic by infiltration will transform to $CaCO_3$ on exposure to moisture and the resulting volume change will remove the adjacent HA grains resulting in the faceted damage. In addition the TetCP on the surface formed by reaction of HA with CaO would dissolve adding to the release of calcium into the saline and the surface damage.

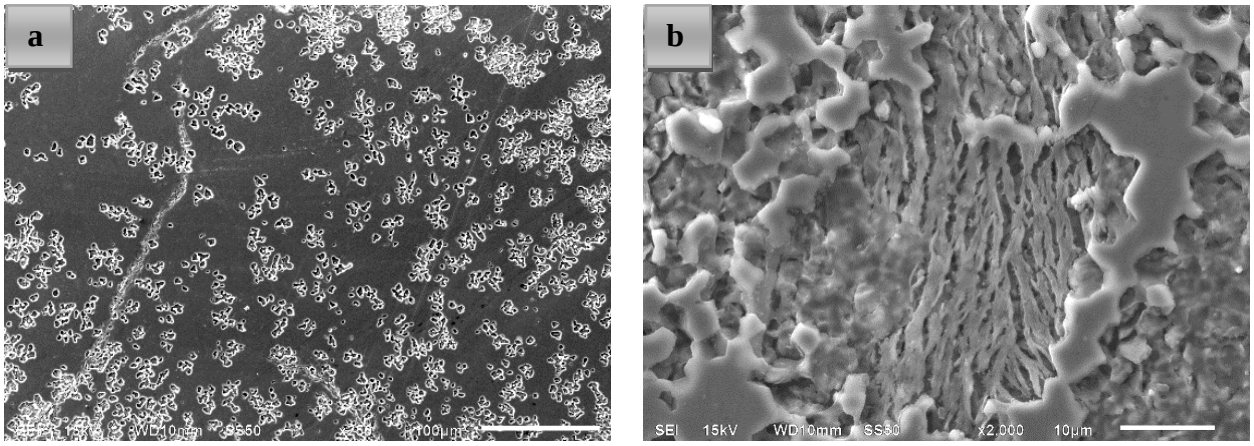

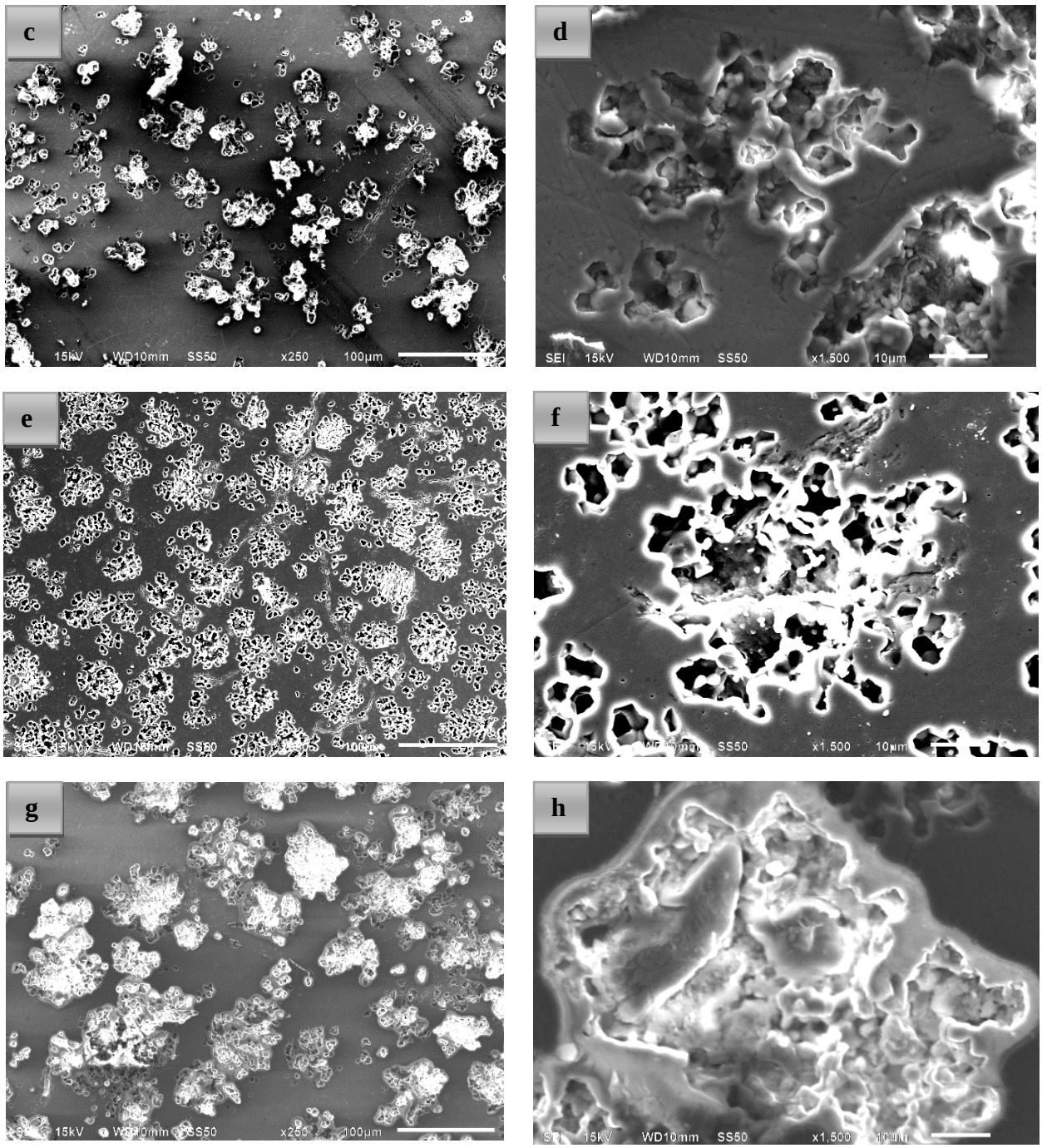

Figure 6.7 SEM images of 5MHA after the solubility test, where a, c, e, g represent 1-hour, 3-day, 1-week, 4-week figures respectively in low magnification, and b, d, f, h are corresponding figures in large magnification.

Different and more diverse morphologies were observed on the surface of 5M1h compared to pure HA, within the interior of the damage as shown in Figure 6.7b, Strip-like, features and more glassy amorphous-like features co-exist with the damage. These morphologies seem to have covered the grains of the ceramic that were exposed when the damage formed at early soak times. These morphologies are thought to suggest precipitation inside the damage, again due to the local calcium and phosphorous concentrations being higher than the solution as a whole.[81]

Such big differences in the damage population compared to the HA must be caused by the heterogeneous distribution of calcium oxide and TetCP introduced in the ceramic by impregnation, the evidence for which has already been confirmed by XRD. It is interesting that after 3-day immersion the stripe-like layers inside the damage are less commonly found and the depth of the damage is increased. Figure 6.8(a) shows that the damage area fraction on the surface does not change significantly between 1 hour and 3 days but does increased from 3 days to 1 week and then show no significant increase from 2 to 4 weeks. Figure 6.8(b) shows that there is an increase in the weight loss when there is an increase in the damage area fraction between 3 days and 1 week but the correlation is not strong given the error bars on the results. However in general, there is an increase in damage area fraction over 4 weeks of immersion and there is a weight loss in the sample occurring over the same time frame. After 4 weeks there is again signs of precipitation inside the damage as shown in Figure 6.7h where precipitates even fill the damage.

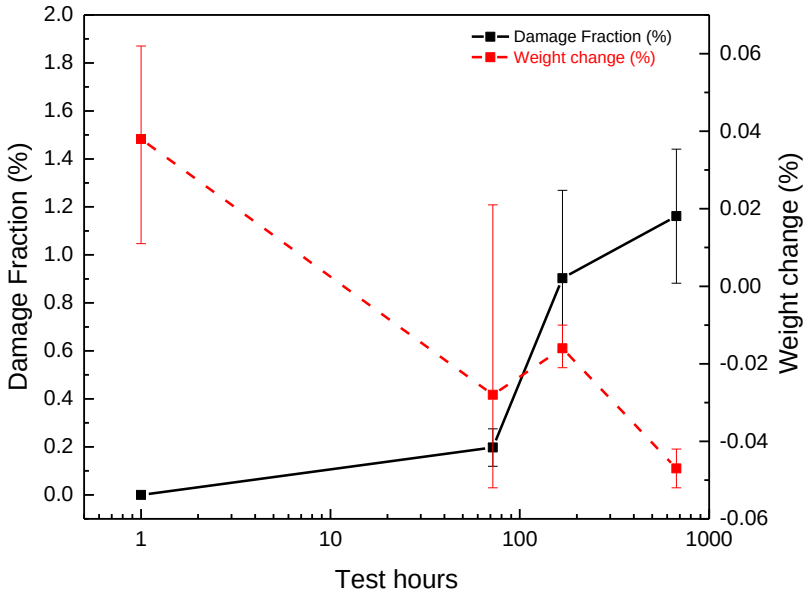

(a) HA samples

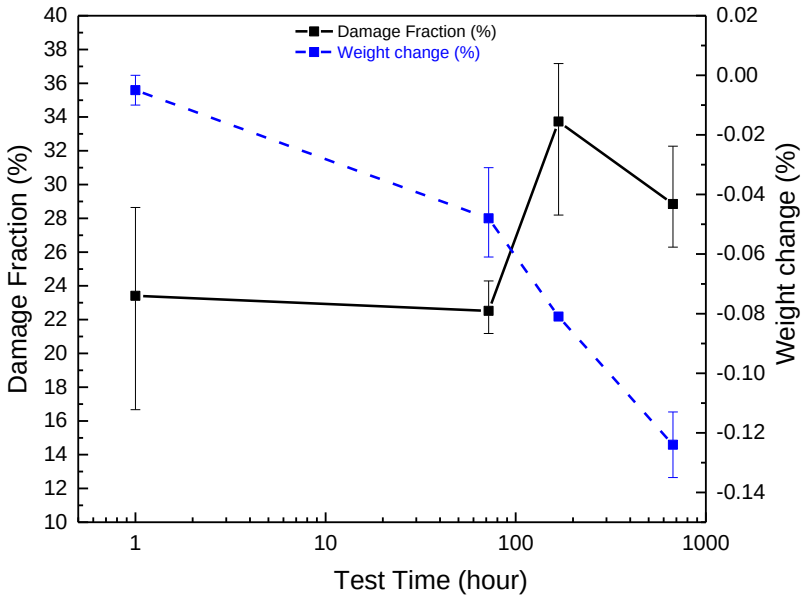

(b) Damage fractions and weight changes of 5MHA

Figure 6.8 Damage fraction combined with weight change of polished samples of HA and 5M infiltrated samples.

Hence, in case of 5MHA, the damage area fraction increases rapidly to 24% during the initial hour of soaking and the damages contained evidence of precipitation that occur only in the damages. Then the precipitates appear to re-dissolve and the damages deepen exposing grains in the interior of the ceramic. Between 3 days to 1 week there is another increase in the surface area of damage and then finally after 1 week the surface area damage remains stable and the damage in the 4 week sample is again filled with precipitation. In general, there is a decrease in weight of the samples during 4 weeks but no correlation with the discontinuous increase in the area fraction of damage.

6.4.3 Mixed HAs

As mentioned before, we designed the mixed HAs to have 5wt% and 10wt% of $CaCO_3$ in the powder respectively and assumed the mixing will lead to uniform distribution of the second phase in the ceramic, unlike the infiltrated ceramic and the overall Ca/P mole ratios will be 1.76 and 1.85 respectively. There is no known phases that have Ca/P molar ratios between that of pure HA at 1.67 and that of TetCP at 2.0. Therefore one would expect the phase distribution would be a mixture of HA and TetCP if equilibrium is established. However, it is possible that CaO and $CaCO_3$ could be present on the surface if the expected solid state reactions had not gone to completion. Returning to the XRD analysis of the sample surface before immersion showed 38% TetCP and 57% TetCP on the surface of the 5wt%$CaCO_3$ sample and the surface of the 10wt% $CaCO_3$ sample respectively. There is a minor amount of $CaCO_3$ on the surface of the 5wt% $CaCO_3$ but non on the surface of the 10wt% $CaCO_3$.

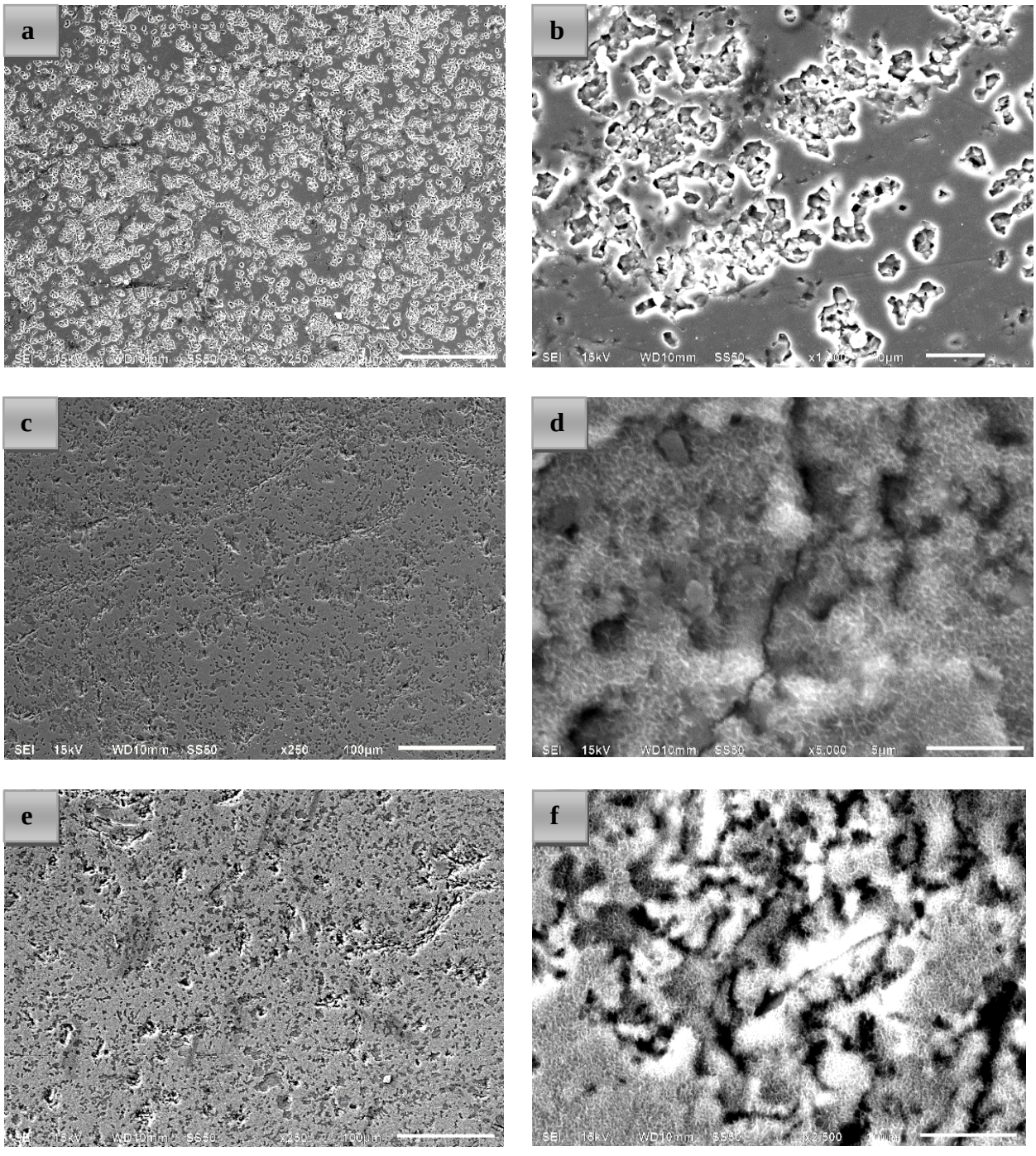
a
b
c
d
e
f
SEI 15kV WD10mm SS50 x250 100µm
SEI 15kV WD10mm SS50 x1,000 10µm
SEI 15kV WD10mm SS50 x250 100µm
SEI 15kV WD10mm SS50 x5,000 5µm
SEI 15kV WD10mm SS50 x250 100µm
SEI 15kV WD10mm SS50 x2,500 10µm

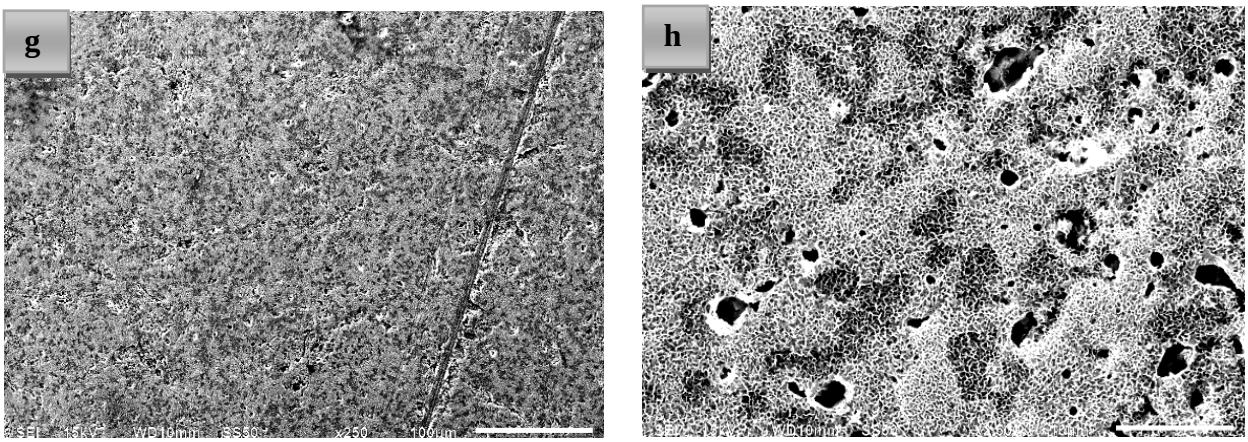

Figure 6.9 SEM images of 5WTHA after the solubility test, where a, c, e, g represent 1-hour, 3-day, 1-week, 4-week figures respectively in low magnification, b, d, f, h are corresponding figures in large magnification.

One-hour immersion of 5WTHA in in TBS gives surface damage similar to that on the infiltrated sample, Figure 6.9a. The damage fraction in this circumstance was measured to be around 28%, a little more than that of the infiltrated samples. New amorphous phase seems to have been formed on the surface of 5WTHA after 3 days and this phase covered the damage area making us difficulty to precisely measure the damage fraction. The original polished surface is now decorated with layer of needle-like precipitates. This needle-like layer was also observed by Hyakuna and et al [82], who also reported that similar precipitate morphologies took around 1 to 2 days to form on HA. In our case, 3 days are long enough to allow this happen. This new formed phase was identified to be a protective carbonated HA layer[78,82]. which would limit the accessibility of solution to the original surface[83]. In addition, since the layer may restrict diffusion form the liquid to the ceramic surface. With increasing time the precipitated surface layer appear to thicken as shown in Figure 5.9h. Interestingly XRD of the surface after 4 weeks of immersion shows that the surface is now HA with minor amounts of $CaCO_3$ and $Ca(OH)_2$ with no TetCP detected.

For the 10wt% mixed samples, the result after 1-hour of saline treatment shows a much higher damage area fraction up to 60%. Therefore, over half of the surface has been removed, as seen in Figure 6.10a. The damages become larger and seem to be connected on the surface. But after 3 days the appearance of the surface has completely changes. The former needle-like precipitates were not found, instead a new amorphous looking layer was formed, as shown in Figure 6.10c and d. The result of EDS suggested that the layer is a carbonated calcium phosphate. A study of TetCP[84] pointed out that the hydrolysis of TetCP in water to form HA and calcium hydroxide will be slowed down due to the formation of this thin HA layer around the particles, the fact of which correlates very well with the occurrence of $Ca(OH)_2$ in XRD result. The morphology of the layer did not seem to change in a significant way with increasing immersion time after 1 week for 10WTHA although the layer may not be as thick at the longer immersion time.

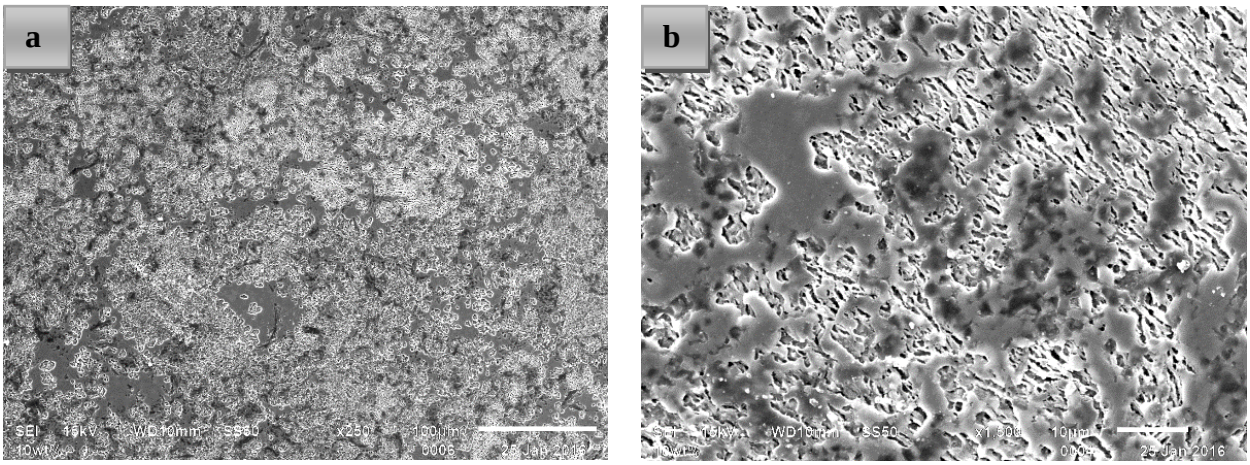

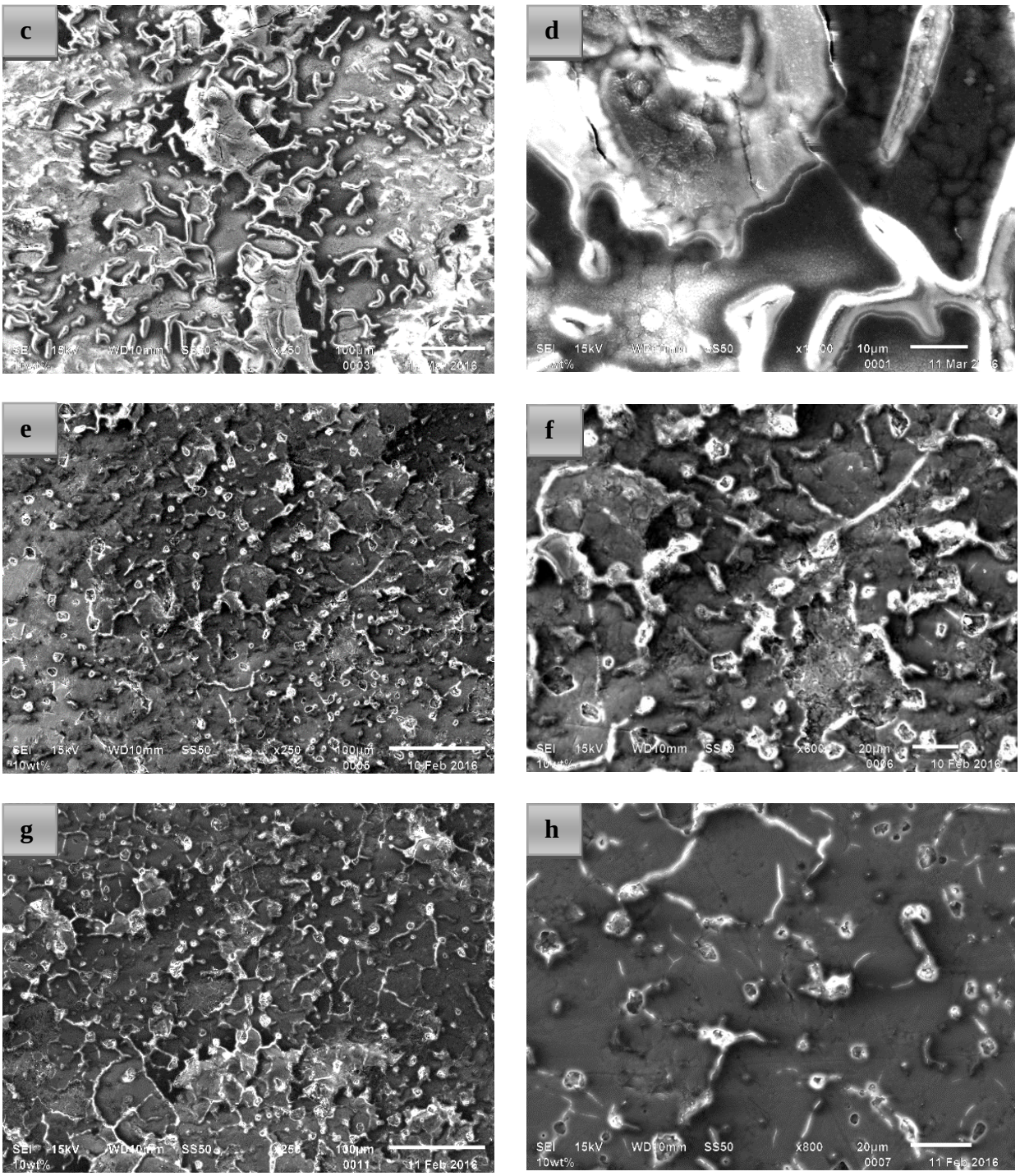

Figure 6.10 SEM images of 10WTHA after the solubility test, where a, c, e, g represent 1-hour, 3-day, 1-week, 4-week figures respectively in low magnification, b, d, f, h are the corresponding figures in large magnification.

Figure 6.11 shows other images of the surface layer on the samples immersed for 3 days and 4 weeks. Other surface layer morphologies were observed so no one layer morphology covered the whole surface of the samples. On the edge of the samples, the morphologies already observed on the HA and 5MHA samples could be found as well. This suggest that the local physiochemical conditions are different at different locations on the sample surface. The different precipitate layers on the 5WTHA and 10WTHA samples and the extent to which the layer covers the surface on the 10WTHA could explain the differences observed in the weight change during immersion. In particular the precipitation on the 10WTHA is responsible for the only consistent weight gain during immersion. The layer forms quickly and may mediate the further damage of the underlying surface. It appears that the layer does not continue to accumulate after 3 days may be re-dissolving into the saline at longer immersion times (Figure 6.10c compared to e and g), leading to a weight loss (Figure 6.5).

Therefore, as far as mixed samples are concerned, the early formation of the surface precipitated phase made surface analysis of the damage difficult after 1 hour. The precipitate are thought to be due to the surface reactions proposed by Hyakuna and et al[71]. There is no one layer morphology covered the whole surface, suggesting that the precipitates are influenced by local physiochemical conditions.

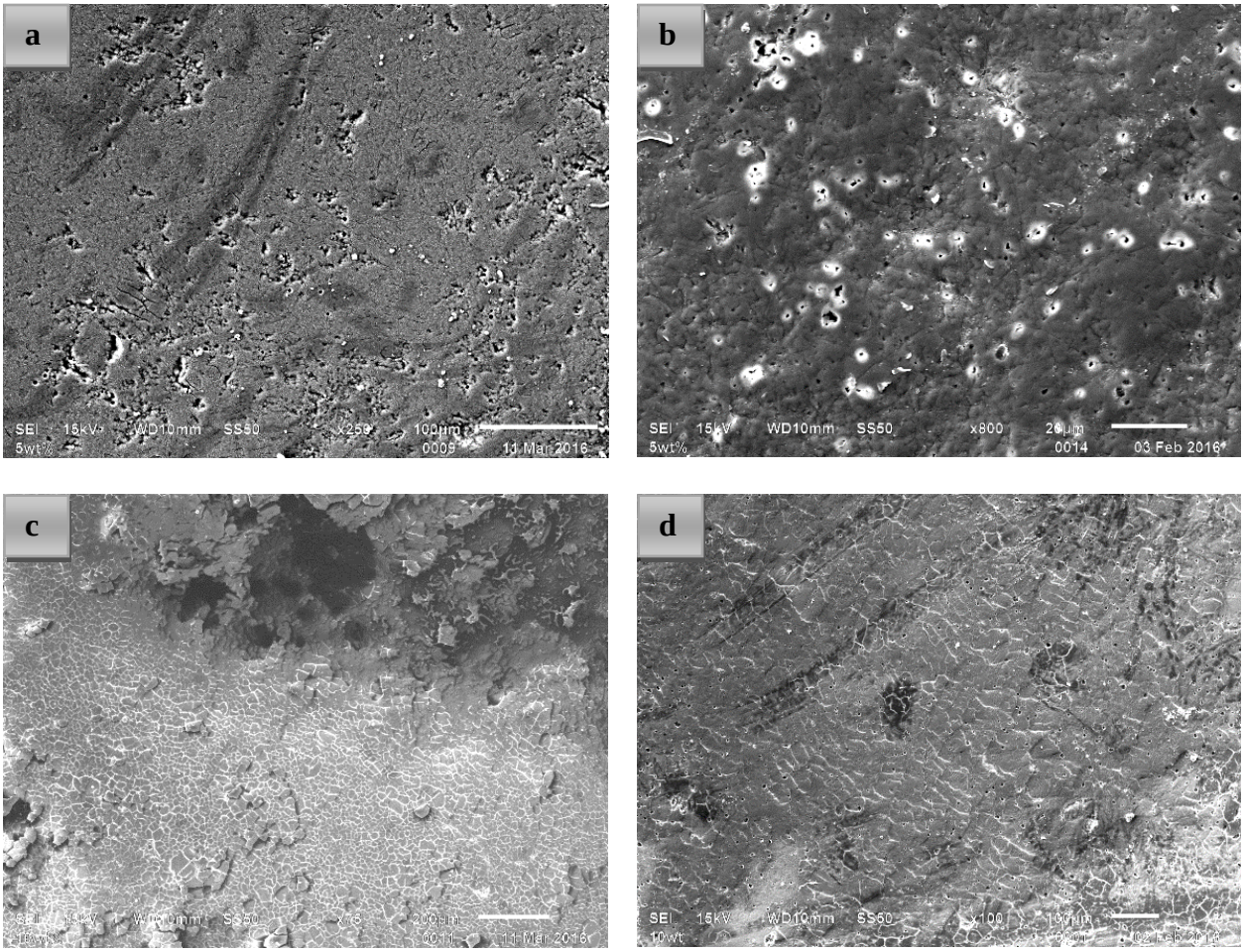

Figure 6.11 Complementary pictures of other captured layers in 5WTHA and 10WTHA, where a, c represent 3 days, b, d 4 weeks.

Since the mixed samples suffer from surface precipitation after 1 hour this is the only time point at which the effect of processing conditions on damage area fraction. This comparison is shown in Figure 6.12. Mixed samples without a doubt have larger damage areas, especially for the 10wt% mixed samples which has almost triple the area fraction damage compared to the infiltrated specimens 5MHA. There is also a large difference between the two mixed HA conditions, where the damage area fraction of 10WTHA is two times larger than that of 5WTHA. It is clear that the fraction of highly soluble phases within the pellet causes these differences. In

the scope of this study, these phases are calcium carbonate and TetCP. Looking back to the XRD result, these two phases before the solubility test occupy 42wt%, 57wt%, and 25wt% for 5WTHA, 10WTHA, and 5MHA, respectively. These roughly correlate with the area fraction of damage after 1 hour but not strictly. The reason for this is not known and further work is required, such as the XRD result of samples exposure to saline for 1 hour, 3 days. One issue that must be remembered is that infiltration creates high concentration of the second phase near the surface of the ceramic that may not be representative of the interior.

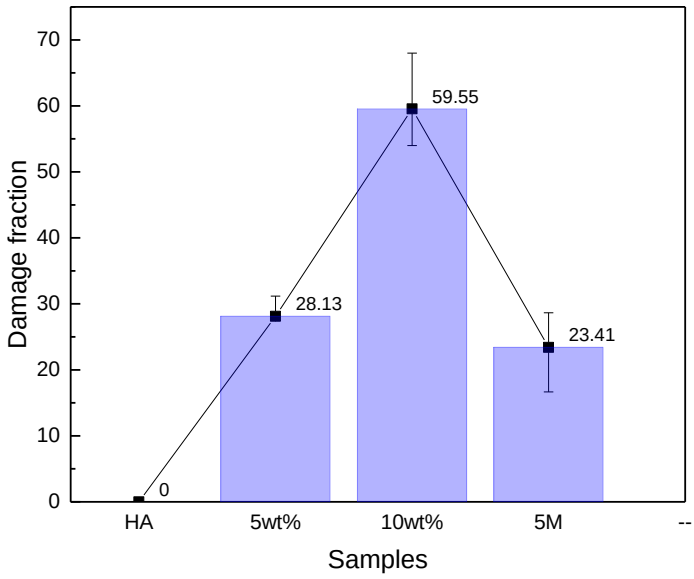

Figure 6.12 Damage fractions of one-hour exposure to TBS of all prepared samples

7.0 CONCLUSIONS

1. The calcium-rich HA made by infiltration did not show densification behavior that was significantly different from HA. The calcium rich HA made by mixing showed lower density at all the sintering times used at 1300℃. The effect was more noticeable for 10wt%$CaCO_3$ than for 5wt%$CaCO_3$ to the extent that open porosity is expected in the 10wt%$CaCO_3$ samples.
2. The extra calcium incorporated into the samples by infiltration and mixing caused the formation of second phases on sintering. In particular TetCP is formed in the samples and small amounts of $CaCO_3$.
3. Exposure to saline caused a lot of surface damage within the first hour for incorporated samples. The area fraction of surface damage did roughly correlate with the measured fraction of the calcium rich phases but not strictly.
4. The 10wt%$CaCO_3$ sample gained weight during the immersion which coincided with the appearance of a surface layer thought to be associated with precipitation.
5. The infiltrated samples lost weight during immersion and the surface damage which appeared very early deepened at longer times. Some precipitation was found within the surface damage but this was more limited.

8.0 FUTURE WORK

While some general trends have been observed for the first time more study is required to be able to determine the clear relationships between the formation of the calcium rich phases, the weight change of the sample and the character of the surface damage. Therefore the following experiments are proposed:

1) More time points and calcium rich phase fractions should be investigated to clearly understand the correlation between the phase fraction of the calcium rich phase and the extent of damage at short immersion times.
2) More experiments should be conducted at time longer than 4 weeks to see if there are long term weight gains in the mixed samples and the weight losses in the infiltrated samples.
3) The chemical composition of the saline should be tested for each time point to see if it correlates with damage formation and surface precipitation.
4) The saline should be replaced periodically during the immersion test to see if this can be used to deepen the surface damages without surface precipitation that is expected to slow down the growth of the damage.
5) Similar experiments should be conducted on single phase materials of TetCP and $CaCO_3$. Both of these materials have been to culture bone marrow cells in the past but the biocompatibility of hematopoietic stem cells with these ceramics have yet to be conducted.

6) When incorporating such high content of CaO into HA, experiment of decreasing temperature to around 1000℃ to 1200℃ right after sintering should be conducted to allow the decomposition of TetCP into HA and CaO occur. Then the solubility tests should be repeated to see if the layer formation would be avoided.

BIBLIOGRAPHY

[1] Finkemeier, C. G. (2002). Bone-grafting and bone-graft substitutes. J Bone Joint Surg Am, 84(3), 454-464.

[2] Hulbert, S. F., Bokros, J. C., Hench, L. L., Wilson, J., and Heimke, G. (1986). Ceramics in clinical applications, past, present and future. High Tech Ceramics.(Part A), 189-213.

[3] Williams, D. F. (1985). The biocompatibility and clinical uses of calcium phosphate ceramics. Biocompatibility of tissue analogs, 2, 43-6.

[4] Tonelli, F. M., Santos, A. K., Gomes, D. A., da Silva, S. L., Gomes, K. N., Ladeira, L. O., and Resende, R. R. (2012). Stem cells and calcium signaling. InCalcium Signaling (pp. 891-916). Springer Netherlands.

[5] https://en.wikipedia.org/wiki/Hematopoietic_stem_cell_niche

[6] "Cell Therapy". American Cancer Society. 1 November 2008. Retrieved 15 September 2013.

[7] Lefrère, J. J., Berche, P. (2010, March). La thérapeutique du docteur Brown-Séquard. In Annales d'Endocrinologie (Vol. 71, No. 2, pp. 69-75). Elsevier Masson.

[8] Starzl, T. E. (2000). History of clinical transplantation. World journal of surgery, 24(7), 759-782.

[9] Mimeault, M., Hauke, R., Batra, S. K. (2007). Stem cells: a revolution in therapeutics – recent advances in stem cell biology and their therapeutic applications in regenerative medicine and cancer therapies. Clinical Pharmacology & Therapeutics, 82(3), 252-264.

[10] Thomson J.A., Itskovitz-Eldor J., Shapiro S.S., Waknitz M.A., Swiergiel J.J., Marshall V.S., Jones J.M. (1998). "Blastocysts Embryonic Stem Cell Lines Derived from Human". Science 282 (5391): 1145–1147.

[11] Ratajczak M.Z., Machalinski B., Wojakowski W., Ratajczak J., Kucia M. (2007). "A hypothesis for an embryonic origin of pluripotent Oct-4(+) stem cells in adult bone marrow and other tissues". Leukemia 21(5): 860–7

[12] "Me too, too – How to make human embryonic stem cells without destroying human embryos". The Economist. 22 November 2007.

[13] Barrilleaux B, Phinney D.G., Prockop D.J., O'Connor K.C. (2006). "Review: ex vivo engineering of living tissues with adult stem cells". Tissue Eng. 12 (11): 3007–19

[14] Takahashi, K; Yamanaka, S (2006). "Induction of pluripotent stem cells from mouse embryonic and adult fibroblast cultures by defined factors". Cell 126 (4): 663–76.

[15] Saltzman, W. M. (2004). Tissue engineering: engineering principles for the design of replacement organs and tissues. Oxford university press.

[16] http://www.doitpoms.ac.uk/tlplib/bones/structure.php

[17] http://training.seer.cancer.gov/anatomy/skeletal/tissue.html

[18] https://en.wikipedia.org/wiki/Bone_marrow

[19] Gordana Vunjak-Novakovic, Nina Tandon, Amandine Godier, Robert Maidhof, Anna Marsano, Timothy P. Martens, and Milica Radisic. Tissue Engineering Part B: Reviews. April 2010, 16(2): 169-187. doi:10.1089/ten.teb.2009.0352.

[20] Nature Bone Marrow Transplantation (Nature Publishing Group) – specialist scientific journal with articles on bone marrow biology and clinical uses.

[21] Cooper, B (2011). "The origins of bone marrow as the seedbed of our blood: from antiquity to the time of Osler"(PDF). Baylor University Medical Center Proceedings 24 (2): 115-8. PMC 3069519. PMID 21566758.

[22] Mehta, P. (2010). Hematopoietic Stem Cell Biology. JAMA, 304(18), 2067-2071.

[23] Harrison, K. L. (1979). "Fetal Erythrocyte Lifespan". Journal of Paediatrics and Child Health 15 (2): 96–97. Harrison, K. L. (1979). Fetal erythrocyte lifespan. Journal of Paediatrics and Child Health, 15(2), 96-97.

[24] https://www.stemcell.ucla.edu/blood-hematopoietic-stem-cells-hsc

[25] Shang, Q., Wang, Z., Liu, W., Shi, Y., Cui, L., Cao, Y. (2001). Tissue-engineered bone repair of sheep cranial defects with autologous bone marrow stromal cells. Journal of Craniofacial Surgery, 12(6), 586-593.

[26] https://en.wikipedia.org/wiki/Scaffolding

[27] https://en.wikipedia.org/wiki/Tissue_engineering#Scaffolds

[28] O'brien, F. J. (2011). Biomaterials & scaffolds for tissue engineering. Materials Today, 14(3), 88-95.

[29] Nerem, R. M. (2006). Tissue engineering: the hope, the hype, and the future. Tissue engineering, 12(5), 1143-1150.

[30] Fuchs, S., Jiang, X., Schmidt, H., Dohle, E., Ghanaati, S., Orth, C., and et al. (2009). Dynamic processes involved in the pre-vascularization of silk fibroin constructs for bone regeneration using outgrowth endothelial cells. Biomaterials, 30(7), 1329-1338.

[31] Daculsi, G. (1998). Biphasic calcium phosphate concept applied to artificial bone, implant coating and injectable bone substitute. Biomaterials, 19(16), 1473-1478.

[32] Jarcho M. Calcium phosphate ceramics as hard tissue prosthetics. Clin Orthop Rel Res 1981; 157: 259–78.

[33] De Groot K. Bioceramics of calcium phosphate. Boca Raton, Fl: CRC Press; 1983.

[34] Vallet-Regi, M., Gonz áez-Calbet, J. M. (2004). Calcium phosphates as substitution of bone tissues. Progress in Solid State Chemistry, 32(1), 1-31.

[35] Dorozhkin, S. V. (2010). Bioceramics of calcium orthophosphates. Biomaterials, 31(7), 1465-1485.

[36] Dorozhkin, S. V. (2012). Biphasic, triphasic and multiphasic calcium orthophosphates. Acta biomaterialia, 8(3), 963-977.

[37] http://www.algaeinstitute.com/hydroxyapatite.html

[38] http://electronicstructure.wikidot.com/cation-substitutions-in-hydroxyapatite

[39] Monma H, Goto M. Behavior of the alpha-beta phase transformation in tricalcium phosphate. Yogyo Kyokai Shi 1983; 91:473–5.

[40] M.J. Buerger, 'Crystallographic aspects of phase transformations', R. Smoluchowski, J.E. Meyer, W.A. Weyl (Eds.): 183–211, Phase transformations in solids, John Wiley, New York (1951).

[41] Carrodeguas, R. G., De Aza, S. (2011). α-Tricalcium phosphate: Synthesis, properties and biomedical applications. Acta biomaterialia, 7(10), 3536-3546.

[42] Driessens, F. C. M., Verbeeck, R. M. H. (1988). Relation between physico-chemical solubility and biodegradability of calcium phosphates. Implant materials in biofunction, Advances in biomaterials, Amsterdam: Elsevier, 105-111.

[43] Shinya Nakamura, Takuya Matsumoto, Jun-Ichi Sasaki, Hiroshi Egusa, et al, 'Effect of Calcium Ion Concentrations on Osteogenic Differentiation and Hematopoietic Stem Cell Niche-Related Protein Expression in Osteoblasts', Tissue engineering: Part A,8(16):2467-2473,(2010).

[44] Lam, B. S., Cunningham, C., Adams, G. B. (2011). Pharmacologic modulation of the calcium-sensing receptor enhances hematopoietic stem cell lodgment in the adult bone marrow. Blood, 117(4), 1167-1175.

[45] Bohner, M. (2000). Calcium orthophosphates in medicine: from ceramics to calcium phosphate cements. Injury, 31, D37-D47.

[46] Liu, Y. K., Lu, Q. Z., Pei, R., Ji, H. J., Zhou, G. S., Zhao, X. L., and et al. (2009). The effect of extracellular calcium and inorganic phosphate on the growth and osteogenic differentiation of mesenchymal stem cells in vitro: implication for bone tissue engineering. Biomedical materials, 4(2), 025004.

[47] Chow, L. C., Eanes, E. D. (Eds.). (2001). Octacalcium phosphate (Vol. 18). Karger Medical and Scientific Publishers.

[48] Rahaman, M. N. (2007). Sintering of ceramics. CRC press.

[49] W.S. Slaughter, I. Nettleship, M.D. Lehigh, P.P. Tong, A quantitative analysis of the effect of geometric assumptions in sintering models, Acta Mater. 45 (1997) 5077_5086.

[50] J. Bernholc, P. Salamon, R.S. Berry, Annealing of fine powders: initial shapes and grain boundary motion, in: P. Jena, B.K. Rao, S.N. Kahanna (Eds.), Physics and Chemistry of Small Clusters, Plenum Press, New York, NY, 1987, pp. 43_48.

[51] M. Upmanyu, G.N. Hassold, A. Kazaryan, E.A. Holm, Y. Wang, B. Patton, et al., Boundary mobility and energy anisotropy effects on microstructural evolution during grain growth, Interface Sci. 10 (2002) 201_216.

[52] G. Petzow, H.E. Exner, Particle rearrangement in solid state sintering, Z. Metall 67 (1976)611_618.

[53] Olevsky, E. A. (1998). Theory of sintering: from discrete to continuum. Materials Science and Engineering: R: Reports, 23(2), 41-100.

[54] German, R. (2014). Sintering: From Empirical Observations to Scientific Principles. Butterworth-Heinemann.

[55] E. Champion, 'Sintering of Calcium phosphate bioceramics', Acta Biomaterialia,4(9):5855-5875,(2013)

[56] Sawicki, M., Crosby, K., Li, L., Shaw, L. (2012). Sintering of Hydroxyapatite. Biomaterials Science: Processing, Properties and Applications II: Ceramic Transactions, Volume 237, 83-89

[57] A. Ravaglioli and A. Krajewski, "Bioceramics" (Chapman and Hall, London, 1992), p. 57.

[58] B. Locardi, V. E. Pazzaglia, C. Gabbi and B. Profilo, Biomaterials 44 (1993) 437.

[59] R. Z. Legeros and J. P. LEGEROS, in "An Introduction to Bioceramics," edited by L. L. Hench and J. Wilson(World Scientific, Singapore, 1993), p. 139.

[60] Muralithran, G., Ramesh, S. (2000). The effects of sintering temperature on the properties of hydroxyapatite. Ceramics International, 26(2), 221-230.

[61] S. Gottschling, R. Kohl, A. Engel and H. J. Oel, in "Bioceramics: Materials and Applications," edited by G. Fischman, A. Clare and L. Hench (American Ceramic Society, Ohio, 1994), p. 201.

[62] Wang, P. E., Chaki, T. K. (1993). Sintering behaviour and mechanical properties of hydroxyapatite and dicalcium phosphate. Journal of Materials Science: Materials in Medicine, 4(2), 150-158.

[63] Malina, D., Biernat, K., Sobczak-Kupiec, A. (2012). Studies on sintering process of synthetic hydroxyapatite. Acta. Biochim. Pol, 60, 851-855.

[64] Cihlář, J., Buchal, A., Trunec, M. (1999). Kinetics of thermal decomposition of hydroxyapatite bioceramics. Journal of materials science, 34 (24), 6121-6131.

[65] B.R. Marple, D. J. Green, 'Graded compositions and microstructures by infiltration processing', Journal of Materials Science, 28 :4637-4643, (1993)

[66] Scherer, G. W. (1990). Theory of drying. Journal of the American Ceramic Society, 73(1), 3-14.

[67] Hassanin, H., Jiang, K. (2010, January). Infiltration-processed, functionally graded materials for microceramic componenents. In Micro Electro Mechanical Systems (MEMS), 2010 IEEE 23rd International Conference on (pp. 368-371). IEEE.

[68] Jedamzik, R., Neubrand, A., Rödel, J. (2000). Functionally graded materials by electrochemical processing and infiltration: application to tungsten/copper composites. Journal of materials science, 35(2), 477-486.

[69] Honeyman-Colvin, P., Lange, F. F. (1996). Infiltration of porous alumina bodies with solution precursors: strengthening via compositional grading, grain size control, and transformation toughening. Journal of the American Ceramic Society, 79(7), 1810-1814.

[70] Studart, A. R., Gonzenbach, U. T., Tervoort, E., Gauckler, L. J. (2006). Processing routes to macroporous ceramics: a review. Journal of the American Ceramic Society, 89(6), 1771-1789.

[71] Sharifi, S., Shafieyan, Y., Mirzadeh, H., Bagheri-Khoulenjani, S., Rabiee, S. M., and et al. (2011). Hydroxyapatite scaffolds infiltrated with thermally crosslinked polycaprolactone

fumarate and polycaprolactone itaconate. Journal of Biomedical Materials Research Part A, 98(2), 257-267.

[72] Juang, H. Y., Hon, M. H. (1996). Effect of calcination on sintering of hydroxyapatite. Biomaterials, 17(21), 2059-2064.

[73] Elliott, J. C. (2013). Structure and chemistry of the apatites and other calcium orthophosphates. Elsevier.

[74] Carayon, M. T., Lacout, J. L. (2003). Study of the Ca/P atomic ratio of the amorphous phase in plasma-sprayed hydroxyapatite coatings. Journal of Solid State Chemistry, 172(2), 339-350.

[75] LeGeros, R. Z., Parsons, J. R., Daculsi, G., Driessens, F., Lee, D., and et al. (1988). Significance of the Porosity and Physical Chemistry of Calcium Phosphate Ceramics Biodegradation - Bioresorption. Annals of the New York Academy of Sciences, 523(1), 268-271.

[76] Klein, C. P. A. T., Driessen, A. A., De Groot, K. (1984). Relationship between the degradation behaviour of calcium phosphate ceramics and their physical-chemical characteristics and ultrastructural geometry. Biomaterials,5(3), 157-160.

[77] Hing, K. A., Gibson, I. R., Di-Silvio, L., Best, S. M., Bonfield, W. (1998). Effect of variation in Ca:P ratio on cellular response of primary human osteoblast-like cells to hydroxyapatite-based ceramics. In Bioceramics-conference (Vol. 11, pp. 293-296)

[78] Budz, J. A., LoRe, M., Nancollas, G. H. (1987). Hydroxyapatite and carbonated apatite as models for the dissolution behavior of human dental enamel. Advances in dental research, 1(2), 314-321.

[79] Christoffersen, J., Christoffersen, M. R., Johansen, T. (1996). Kinetics of growth and dissolution of fluorapatite. Journal of crystal growth, 163(3), 295-303.

[80] Wang, H., Lee, J. K., Moursi, A., Lannutti, J. J. (2003). Ca/P ratio effects on the degradation of hydroxyapatite in vitro. Journal of Biomedical Materials Research Part A, 67(2), 599-608.

[81] Ducheyne, P., Radin, S., King, L. (1993). The effect of calcium phosphate ceramic composition and structure on in vitro behavior. I. Dissolution. Journal of biomedical materials research, 27(1), 25-34

[82] Hyakuna, K., Yamamuro, T., Kotoura, Y., Oka, M., Nakamura, T., and et al. (1990). Surface reactions of calcium phosphate ceramics to various solutions. Journal of biomedical materials research, 24(4), 471-488.

[83] Mafe, S., Manzanares, J. A., Reiss, H., Thomann, J. M., Gramain, P. (1992). Model for the dissolution of calcium hydroxyapatite powder. *The Journal of Physical Chemistry*, *96*(2), 861-866.

[84] Moseke, C., Gbureck, U. (2010). Tetracalcium phosphate: Synthesis, properties and biomedical applications. *Acta Biomaterialia*, *6*(10), 3815-3823.